

SANDIA REPORT

SAND95-1759 • UC-814

Unlimited Release

Printed September 1997



TL0006040

**SANDIA NATIONAL
LABORATORIES
TECHNICAL LIBRARY****Yucca Mountain Site Characterization Project****Creep Properties of the Paintbrush Tuff
Recovered from Borehole USW NRG-7/7A:
Data Report**

R. J. Martin, J. S. Noel, P. J. Boyd, R. H. Price

Prepared by
Sandia National Laboratories
Albuquerque, New Mexico 87185 and Livermore, California 94550

Sandia is a multiprogram laboratory operated by Sandia Corporation,
a Lockheed Martin Company, for the United States Department of
Energy under Contract DE-AC04-94AL85000.

Approved for public release; distribution is unlimited.

**Sandia National Laboratories**

"Prepared by Yucca Mountain Site Characterization Project (YMSCP) participants as part of the Civilian Radioactive Waste Management Program (CRWM). The YMSCP is managed by the Yucca Mountain Project Office of the U.S. Department of Energy, DOE Field Office, Nevada (DOE/NV). YMSCP work is sponsored by the Office of Geologic Repositories (OGR) of the DOE Office of Civilian Radioactive Waste Management (OCRWM)."

Issued by Sandia National Laboratories, operated for the United States Department of Energy by Sandia Corporation.

NOTICE: This report was prepared as an account of work sponsored by an agency of the United States Government. Neither the United States Government nor any agency thereof, nor any of their employees, nor any of their contractors, subcontractors, or their employees, makes any warranty, express or implied, or assumes any legal liability or responsibility for the accuracy, completeness, or usefulness of any information, apparatus, product, or process disclosed, or represents that its use would not infringe privately owned rights. Reference herein to any specific commercial product, process, or service by trade name, trademark, manufacturer, or otherwise, does not necessarily constitute or imply its endorsement, recommendation, or favoring by the United States Government, any agency thereof, or any of their contractors or subcontractors. The views and opinions expressed herein do not necessarily state or reflect those of the United States Government, any agency thereof, or any of their contractors.

Printed in the United States of America. This report has been reproduced directly from the best available copy.

Available to DOE and DOE contractors from
Office of Scientific and Technical Information
P.O. Box 62
Oak Ridge, TN 37831

Prices available from (615) 576-8401, FTS 626-8401

Available to the public from
National Technical Information Service
U.S. Department of Commerce
5285 Port Royal Rd
Springfield, VA 22161

NTIS price codes
Printed copy: A04
Microfiche copy: A01

SAND95-1759
Unlimited Release
Printed September 1997

Distribution
Category UC-814

**CREEP PROPERTIES of the PAINTBRUSH TUFF RECOVERED FROM
BOREHOLE USW NRG-7/7A: DATA REPORT**

R. J. Martin, J. S. Noel, P. J. Boyd
New England Research, Inc.
White River Junction, Vermont 05001

R. H. Price
YMP Performance Assessment Applications Department
Sandia National Laboratories
P.O. Box 5800
Albuquerque, New Mexico 87185-1325

ABSTRACT

Experimental results are presented for seven creep experiments performed on welded specimens of the Paintbrush tuff recovered from borehole USW NRG-7/7A at Yucca Mountain, Nevada. The measurements were performed at differential stresses of 40, 70, 100, and 130 MPa. The confining pressure and temperature for each of the experiments was 10 MPa and 225 °C respectively. All of the specimens were tested drained, in a room dry condition. All of the experiments were terminated prior to failure. The duration of the experiments range from 2.6×10^6 seconds to 5.9×10^6 seconds. Creep strain is observed for those specimens tested at a stress difference greater than 70 MPa. The rate of strain accumulation increases with stress difference. The strain rate is not constant. A primary creep stage is observed. Secondary creep does not exhibit a constant strain rate, but decreases with increasing time.

This report was prepared for the Yucca Mountain Site Characterization Project. The scientific investigation discussed in this report is covered under the description of work for WBS number 1.2.3.2.7.1.3, QA Grading Report #1.2.3.2.7.1.3, Revision 00. The planning documents that guided this work activity are Site Characterization Plan Section 8.3.1.15.1.3; Study Plan SP-8.3.1.15.1.3, Revision 0; and Work Agreement WA-0090. The information and data documented in this report were collected under a fully qualified QA Program and may be used in the licensing process. The data contained in this report have been submitted on Technical Data Information Form (TDIF) #305513 under Data Tracking Numbers (DTN) SNL02071596001.001.

CONTENTS

<u>Section</u>	<u>Page</u>
ABSTRACT	i
CONTENTS	ii
1.0 INTRODUCTION	1
2.0 EXPERIMENTAL PROCEDURE	1
2.1 Sample Preparation	4
2.2 Compressional and Shear Wave Velocity Measurements	5
2.3 Cylindrical Rock Core Specimens Tested in Triaxial Creep.....	7
2.3.1 Test Apparatus.....	8
2.3.2 System Calibration	14
2.3.2.1 Temperature Gradient in Tuff Specimens	15
2.3.2.2 Correction for Displacement of the Test System	15
2.3.3 Experimental Procedure for Creep Experiments at Elevated Temperature and Pressure	20
2.3.4 Test Performed in Large Load Frame	22
3.0 RESULTS	23
4.0 DISCUSSION.....	34
5.0 REFERENCES	43
APPENDICES	
I: Information from the Reference Information Base.....	44

List of Figures

Figure 1: Stratigraphic and thermal/mechanical units for borehole USW NRG-7/7A .	2
Figure 1 (continued): Stratigraphic and thermal/mechanical units for borehole USW NRG-7/7A	3
Figure 2: Schematic diagram for velocity measurements.....	6
Figure 3: Schematic diagram of creep pressure vessel.....	9
Figure 4: Schematic diagram of the creep apparatus.....	10
Figure 5: Temperature profile along the axis of a tuff specimen.....	16
Figure 6: Displacement plotted as a function of differential stress for a fused quartz specimen.....	18
Figure 7: System corrections for each creep apparatus	19
Figure 8: Axial strain plotted as a function of time for a creep test at 225 °C	25

Figure 9: Stress differences plotted as a function of time for a creep test conducted at 225 °C at a confining pressure of 10 MPa	26
Figure 10: Temperature plotted as a function of time for a creep test at a differential stress of 130 MPa and a confining pressure of 10 MPa	27
Figure 11: Axial strain plotted as a function of time for three creep experiments conducted simultaneously at a confining pressure of 10 MPa and a temperature of 225 °C	29
Figure 12: Stress differences plotted as a function of time for three creep tests conducted at 225 °C and a confining pressure of 10 MPa	30
Figure 13: Temperature plotted as a function of time for three creep experiments conducted simultaneously in independent test systems	31
Figure 14: Axial strain plotted as a function of time for three creep experiments conducted simultaneously in independent test systems	33
Figure 15: Stress difference plotted as a function of time for three creep experiments conducted simultaneously in independent test systems	35
Figure 16: Temperature plotted as a function of time for three creep experiments conducted simultaneously in independent test systems	36
Figure 17: Axial strain plotted vs log time for specimens of welded tuff tested at a confining pressure of 10 MPa and a temperature of 225 °C	37
Figure 18: Axial strain plotted vs log time for a specimen of welded tuff tested at a stress difference of 130 MPa, a confining pressure of 10 MPa and a temperature of 225 °C	38
Figure 19: Axial strain plotted vs log time for a specimen of welded tuff tested at a confining pressure of 10 MPa and a temperature of 225 °C	39

List of Tables

Table 1: Creep tests data summaries	24
---	----

1.0 INTRODUCTION

An integral part of the licensing procedure for the potential nuclear waste repository at Yucca Mountain, Nevada involves the prediction of *in situ* rheology for the emplacement of containers containing radioactive waste. The data used to model the thermal and mechanical behavior of the rock repository and surrounding lithologies require a detailed knowledge of the time dependent strength of the tuff, in particular the welded unit TSw2, the potential repository horizon. In this study, a suite of experiments was performed on cores recovered from the USW NRG-7/7A borehole drilled in support of the Exploratory Studies Facilities (ESF) at Yucca Mountain. USW NRG-7/7A was drilled to a depth of 1,513.4 feet through five thermal/mechanical units of the Paintbrush tuff and terminated in the tuffaceous beds of the Calico Hills. The thermal/mechanical stratigraphy was defined by Ortiz et al. (1985) to group rock horizons of similar properties for the purpose of simplifying modeling efforts. The relationship between the geologic stratigraphy and the thermal/mechanical stratigraphy is presented in Figure 1. The tuff samples at Yucca Mountain have a wide range of welding characteristics (usually reflected in sample porosity), and a smaller range of mineralogy and petrology characteristics. Generally, the samples are silicic, ash-fall and ash-flow tuffs that exhibit large variability in their elastic and strength properties (see Price and Bauer, 1985).

Seven specimens were prepared from cores of USW NRG-7/7A to conduct creep experiments. All of the specimens have a similar porosity and were from the TSw2 thermal/mechanical unit.

2.0 EXPERIMENTAL PROCEDURE

Measurements were performed on seven specimens prepared from core recovered from borehole USW NRG-7/7A. The specimens were from Topopah Spring tuff.

USW NRG-7/7A
Stratigraphic and Thermal/Mechanical Units Summary
0 - 881 Feet

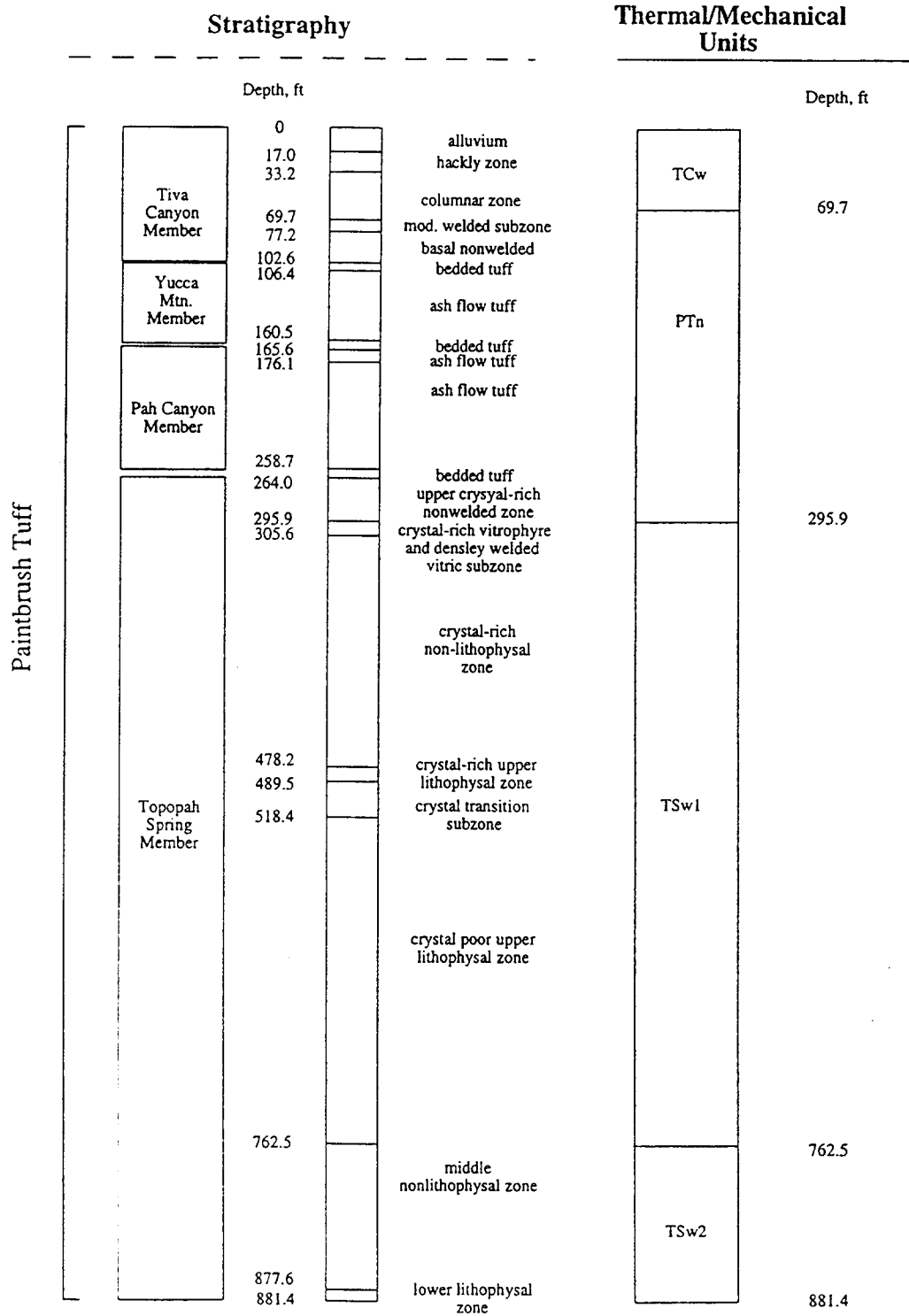


Figure 1: The correlation between the stratigraphic and thermal/mechanical units for borehole USW NRG-7/7A at Yucca Mountain, Nevada (Kicker et al.).

USW NRG-77A
Stratigraphic and Thermal/Mechanical Units Summary
881 - 1513 Feet

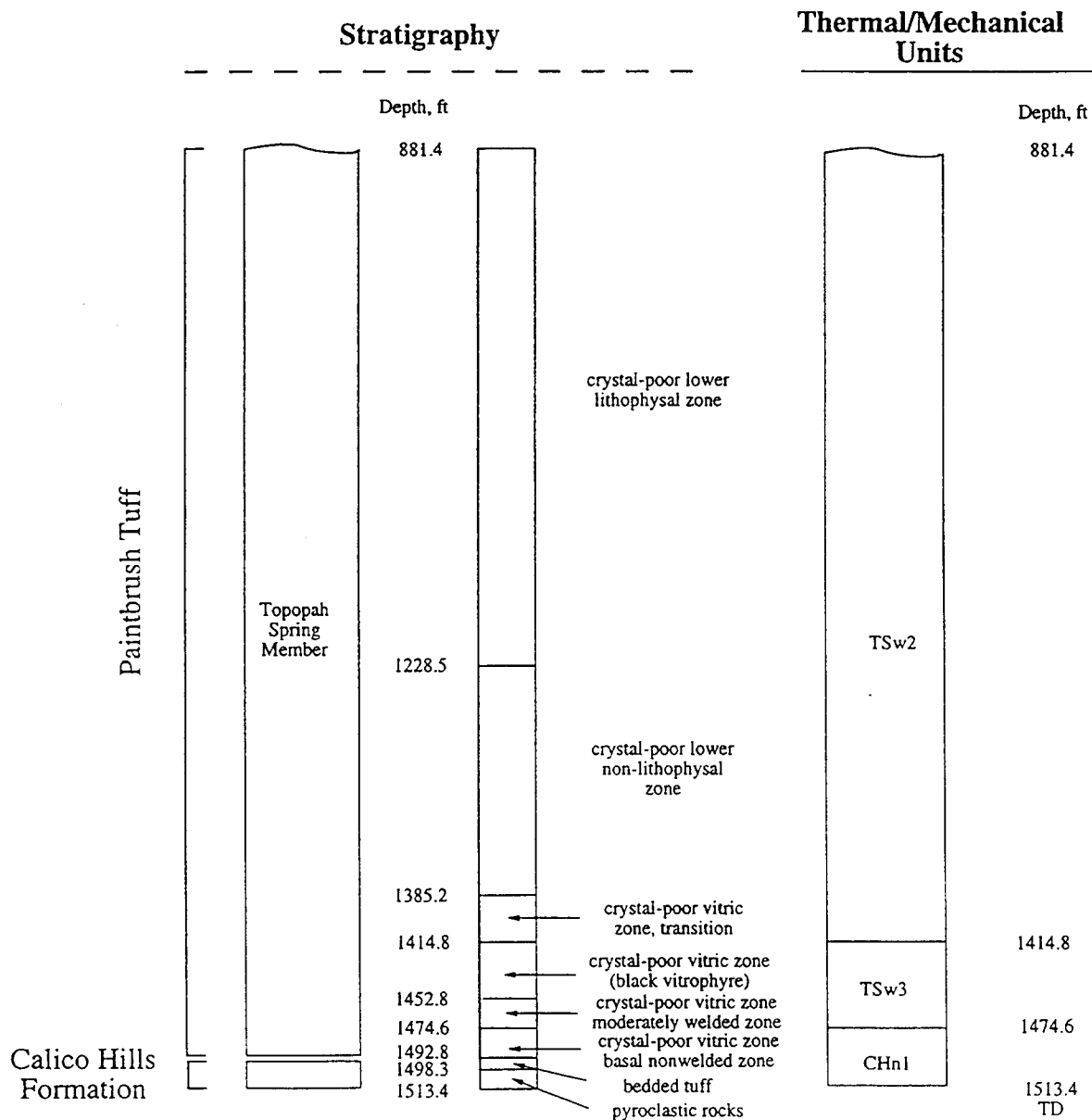


Figure 1 (continued): The correlation between the stratigraphic and thermal/mechanical units for borehole USW NRG-77A at Yucca Mountain, Nevada (Kicker et al.).

The detailed lithostratigraphy incorporates the subtle changes in composition and microstructure. The specimens for this study were from five lithostratigraphic facies:

Tptpmn - crystal poor, middle non lithophysal zone,

Tptpln - crystal poor, lower non lithophysal zone.

Each specimen is a ground, right circular cylinder 50.8 mm in diameter and 101.6 mm in length. The length and diameter have a tolerance of ± 0.125 mm. The ends of the specimens are parallel to within 0.025 mm. "As tested" bulk densities are measured prior to testing (specimens were not oven dried prior to testing). The average grain density is determined with the water pycnometry technique (see Boyd et al., 1994; Martin et al., 1995).

2.1 Sample Preparation

The dimensions of the specimens are checked and verified according to the Sandia National Laboratories (SNL) Technical Procedure (TP) 51 entitled "Preparing Cylindrical Samples, Including Inspection of Dimensional and Shape Tolerances."

The prepared specimens are labeled and stored in containers until the measurement sequence is initiated.

The general measurement sequence for each specimen is given below:

Dimensions measurement

Specimen description

Bulk density measurement in an "as tested" condition

Compressional and shear wave velocities in the "as tested" condition

Creep testing at a confining pressure of 10 MPa, and a temperature of 225 °C

Description of post test condition of the specimen

2.2 Compressional and Shear Wave Velocity Measurements

Compressional and shear wave velocities are measured on right circular cylinders with a nominal length to diameter ratio of 2:1. The velocities are measured in a benchtop apparatus for “as tested” moisture conditions and at ambient temperature.

The compressional and shear wave velocity measurements are used for two main purposes. First, a measure of the specimen anisotropy can be directly obtained by comparing the compressional and shear wave velocities measured both parallel and normal to the core axis. Second, compressional and shear wave velocity data, combined with the density of the specimen, are used to compute dynamic Young’s modulus and Poisson’s ratio.

A self-contained ultrasonic measuring system is used to perform the velocity measurements. A tuff specimen is placed between a matched set of ultrasonic transducers. One transducer serves as the source; the second as the receiver (Figure 2). The travel time through the rock is divided by the sample length to compute the velocity.

Each ultrasonic transducer contains one compressional and one or two polarized shear wave elements. For the measurements parallel to the core axis one compressional and two orthogonally polarized shear waves are propagated. For measurements normal to the core axis, one compressional and one polarized shear wave velocity are measured. The polarization direction of the shear wave propagating normal to the core axis is parallel to the axis of the core.

The transducers are constructed using piezoelectric crystals with a resonant frequency of 1 MHz. The multicomponent piezoelectric crystals are bonded to a titanium substrate. Titanium has been selected because it has a good acoustical impedance match both to the rock and to the piezoelectrical crystals. The source crystal is excited with a fast rise time pulse generator. The crystal produces a broad band ultrasonic pulse propagated through

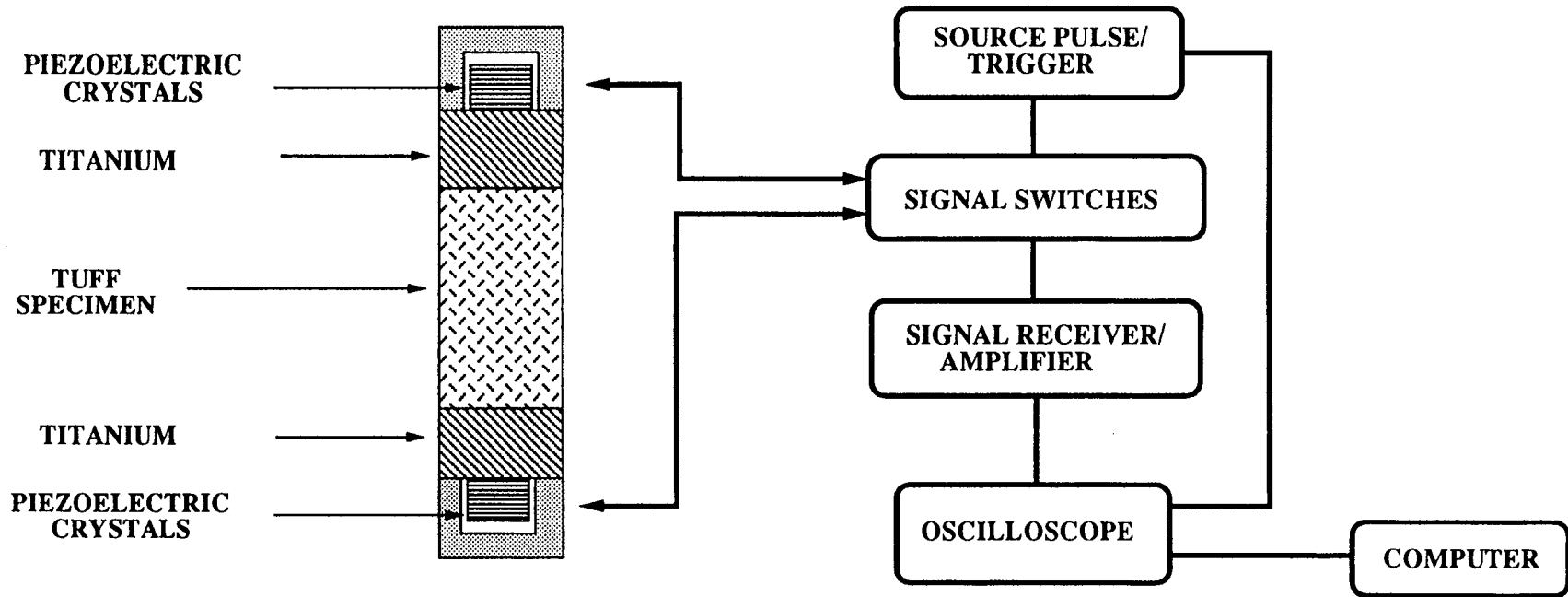


Figure 2: Schematic diagram of the geometry used to measure compressional and shear wave velocities in tuff. The diagram shows the setup for the measurement of velocities parallel to the core axis.

the adjacent titanium substrate, the rock, the titanium at the opposite end of the core, and into the receiver crystal. The received electrical signal is then amplified and filtered through the receiving section of the pulser-receiver and displayed on a digital storage oscilloscope. The signals are amplified, and high pass filtered above 0.3 MHz. The time series displayed on the oscilloscope is then digitized and transferred to a computer for subsequent analysis including picking the first arrival of the compressional and shear wave energy to compute the compressional and shear wave velocities. The total travel times are corrected for the travel time through the titanium end caps prior to calculating the velocities. The accuracy of the travel time is ± 0.02 microseconds.

Pneumatic actuators couple the transducer assemblies in both the axial and radial directions. The stress across the interface for both the matched transducer pairs is identical; this is accomplished by adjusting the loading areas in the pneumatic actuators. The titanium pieces for the radial transducers are concave to mate with the rock surface. Because of the geometry of the interface, only polarizations parallel to the core axis are propagated for shear waves in the radial direction.

2.3 Cylindrical Rock Core Specimens Tested in Triaxial Creep

The creep experiments are performed on right, circular cylinders of TSw2 tuff with a nominal length to diameter ratio of 2 to 1, at a constant confining pressure of 10 MPa, and a temperature of 225 °C. The specimens are jacketed and inserted in a pressure vessel. The confining pressure and temperature are increased to specified conditions. A differential stress is then rapidly applied to the specimen and held constant for the duration of the test. The deformation of the specimen is measured as a function of time. The experiment is terminated at a prespecified time or when the specimen fails. The test procedure used for these measurements is based on ASTM D 4406-93 “Standard Test Method for Creep of Cylindrical Rock Core Specimens in Triaxial Compression”.

ASTM D 4406-93 points out that the moisture content can have a significant effect on the deformation of rock. In fact, theoretical and experimental studies have shown that a key factor in creep of brittle rocks is the water concentration (partial pressure of water) in the pore space surrounding propagating cracks (see Martin et al., 1995). After discussions with representatives of the Department of Energy and the Management and Operations Contractor, it was decided that the tests be performed in a drained condition, beginning with room dry specimens. No attempt was made to maintain the pretest concentration of water in the specimen. Water is expelled from the specimen during initial heating and the water concentration presumably remains constant for the remainder of the test. This condition is similar to that expected in the near-field rock in repository emplacement drifts.

2.3.1 Test Apparatus

Six creep experiments were conducted in the test apparatus described below. One experiment was carried out in the apparatus described previously by Martin et al., (1991).

The creep measurements are conducted in a servo-hydraulic creep testing apparatus. The key features of the system include independent controls for the (1) axial force, producing the differential stress on the sample, (2) confining pressure, (3) pore pressure, and (4) temperature. The creep apparatus is a compact unit designed to handle test specimens up to 50.8 mm in diameter and 120 mm in length, at confining pressures to 35 MPa, pore pressures to 35 MPa, and temperatures to 225 °C. The system, as configured for these experiments, exerts a maximum axial force on the specimen of 640 kN.

A schematic diagram of the pressure vessel is shown in Figure 3; the configuration of the entire system is shown in Figure 4. Since the apparatus design is specifically adapted to conduct creep measurements on specimens 50.8 mm in diameter, it is possible

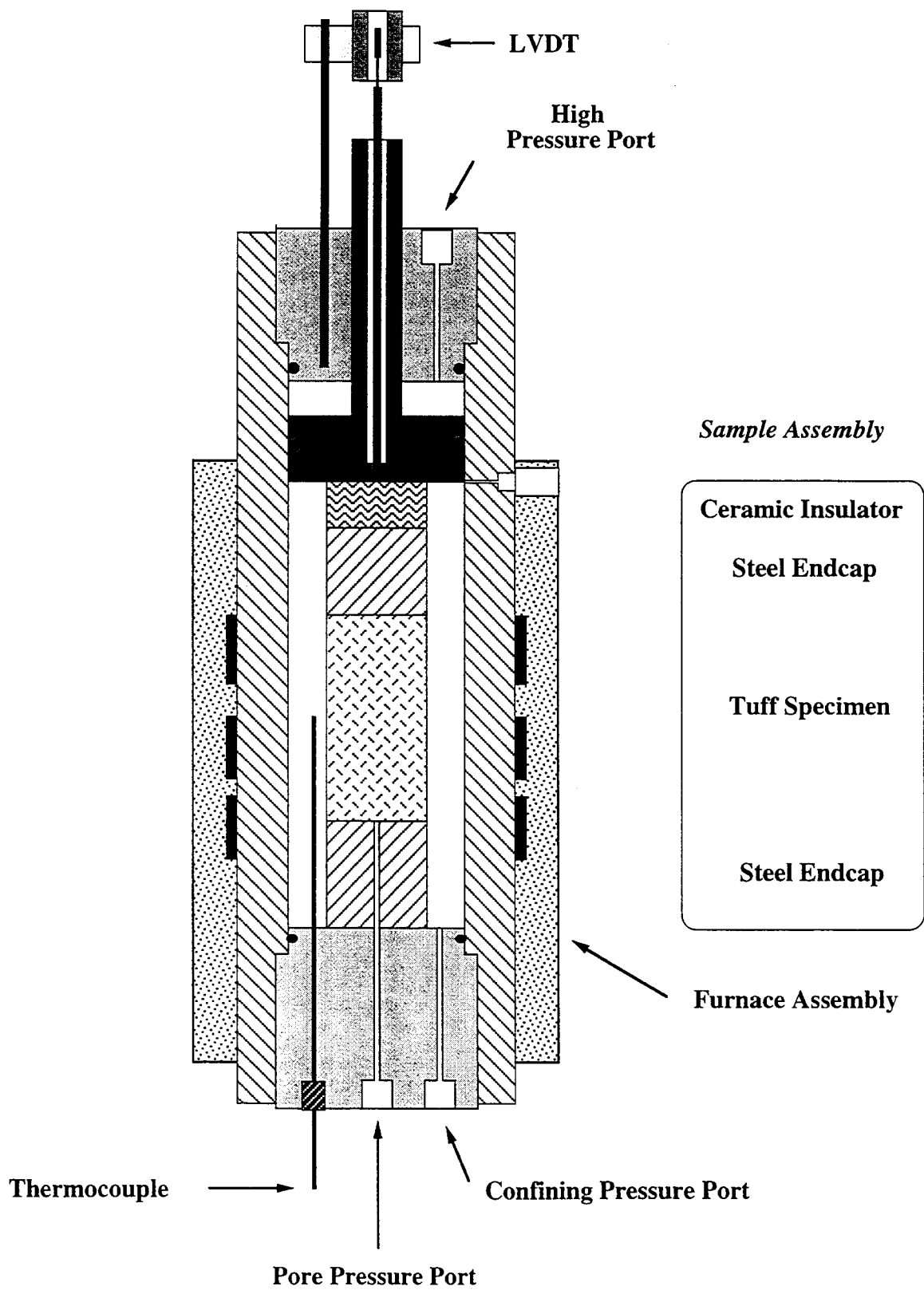


Figure 3: Schematic of the pressure vessel, sample assembly, and loading configuration for the test apparatus used to perform creep measurements on tuff.

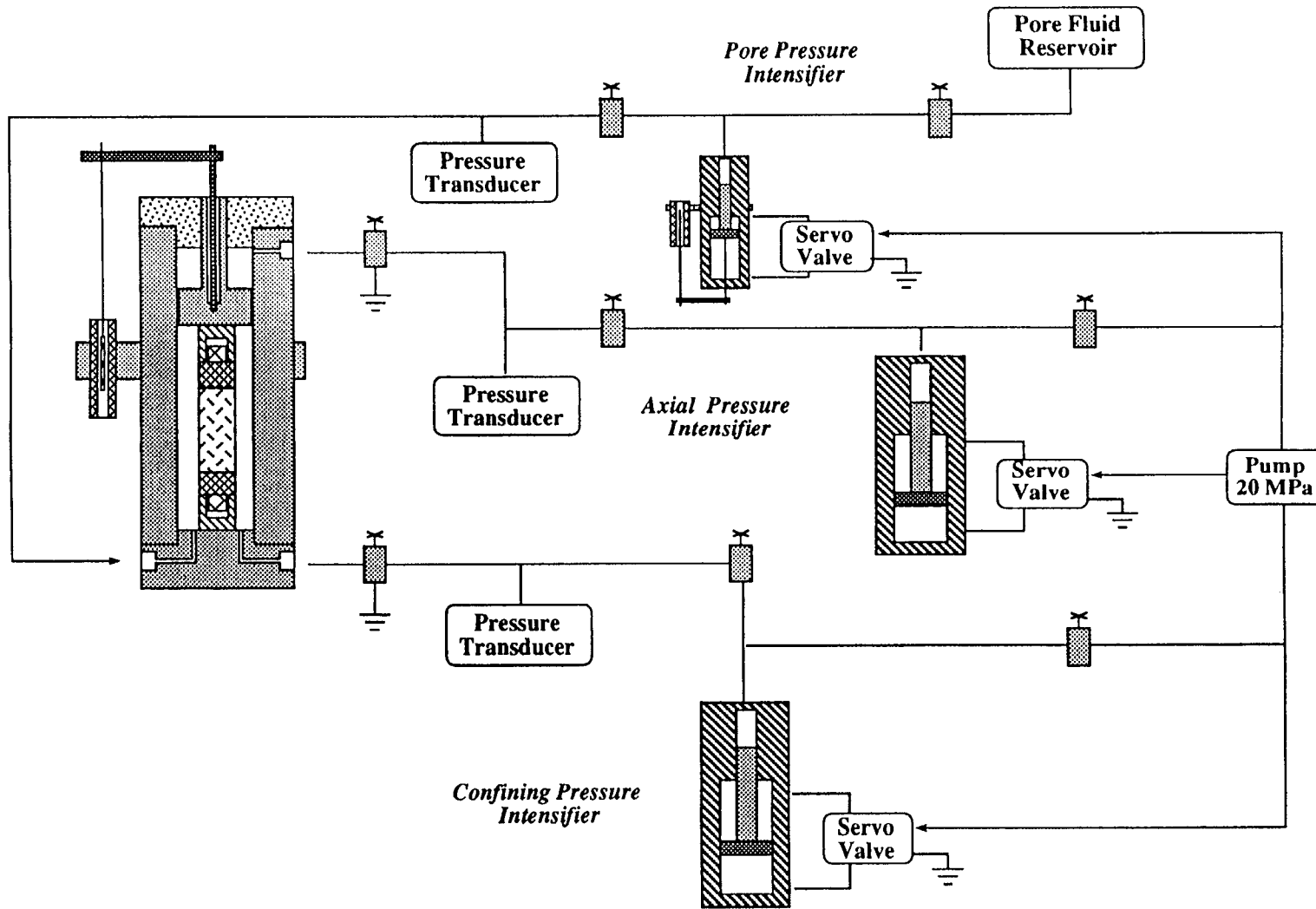


Figure 4: Schematic diagram of the apparatus used in the creep measurements of tuff at elevated temperatures and pressures.

to use an extremely compact test apparatus. The system consists of a pressure vessel divided into two chambers separated with a moveable piston. The specimen resides in the low pressure chamber. This chamber exerts confining pressure on the specimen. The higher pressure, in the upper chamber, moves the piston in contact with the sample assembly. The force exerted on the sample is given by

$$F = P_a A_a - P_c A_c - f_s$$

where P_c is the confining pressure, A_c is the area of the piston in the low pressure chamber, P_a is the pressure in the high pressure chamber, A_a is the effective area of the piston in the high pressure chamber, and f_s is the seal friction. Note, with this design, as the confining pressure increases, the maximum differential force that the system can exert on the test specimen decreases. For example, with no confining pressure, a maximum stress of 350 MPa can be applied to a 50.8 mm diameter specimen. Maximum possible stress difference on a specimen with a confining pressure of 20 MPa is 290 MPa.

The seal friction, f_s , is assumed to remain constant and not to reverse direction during an experiment. At a fixed confining pressure, the net force on the piston when it begins to advance is a measure of the seal friction. To eliminate the seal friction from the stress calculation, the stress difference is considered to be zero at the pressure required to initiate movement on the piston (when the piston is not in contact with the specimen). The difference in the pressure to initiate piston displacement and the subsequent increase of pressure to exert a force on the specimen is used to calculate the stress difference.

The pressure vessel is constructed of 4140 tool steel hardened to R_c 35. The threaded closures of the pressure vessels are fabricated from 17-4 stainless steel. The internal moveable loading piston, that separates the two pressure chambers, is titanium. The bore diameter of the vessel is 92.1 mm; the effective bore length is 235 mm. The pressure vessel is rated to 125 MPa.

The system is controlled with three servo-hydraulic intensifiers (Figure 4). Each of

the servo intensifiers maintains the pressure constant to within ± 0.15 MPa. Fluctuations in pressure are due to long term drift in the servo-valve, pressure transducer, and electronics. The confining pressure is generated and controlled with a servo-hydraulic intensifier with an intensification ratio of 1.5 to 1. The feedback for the servo-controller is a Sensotec Model Z/743 pressure transducer. The accuracy of the transducer is ± 0.5 % of its full scale capacity. The pressure rating of the transducer is 35 MPa.

Specimens are tested in either a drained or undrained condition. For this series of tests, the specimens were drained. For the drained condition, the access port in the base plug supporting the sample assembly is vented to the atmosphere. In some instances it may be desirable to test saturated specimens at elevated pore fluid pressure. The pore pressure is generated and maintained with an independent servo-hydraulic intensifier. Fluid is injected into the base of the sample; in most cases, water is used as a pore fluid. The output volume of the pore pressure intensifier is 5.5 cm^3 . The intensification ratio of the intensifier is 16 to 1. The feedback for the servo-controller is provided with a Sensotec Model Z/743 pressure transducer. The pressure transducer has an accuracy of ± 0.5 %; the pressure rating is 35 MPa.

The pressure on the high pressure side of the moveable piston in the test vessel is controlled with an independent servo-hydraulic intensifier. The intensifier has an intensification ratio of 5.6 to 1. The feedback for the servo-amplifier is provided with a Sensotec Model Z/743 pressure transducer. The pressure rating of the transducer is 70 MPa. The accuracy of the transducer is ± 0.5 %.

Tests are conducted at 225°C . The test specimen is heated with an external furnace. The furnace consists of three independent band heaters positioned on the outside of the pressure vessel in such a way as to produce a uniform temperature distribution throughout the test specimen. (Details are presented below in the System Calibration Section.) The three band elements are wired in parallel. The feedback for the temperature controller is a

type J thermocouple mounted on the outside of the vessel near the band heaters. The outside of the vessel is insulated with a 40 mm thick high density fiber insulation. A stainless steel safety shroud is used to protect the entire furnace assembly. The band heaters are controlled with an Omega model CN9000A temperature controller. The controller is adjusted according to the manufacturer's suggested procedure to maintain a temperature at the test specimen of ± 1 °C. A type J thermocouple is located inside the pressure vessel to monitor the temperature at the midpoint of the specimen during an experiment.

The axial strain of the specimen is measured with an external displacement transducer (LVDT). The displacement of the moveable piston inside the pressure vessel is measured with respect to the closure plug for the high pressure chamber of the pressure vessel. The displacement of the piston is continuously monitored throughout the experiment. Since the differential stress, confining pressure, pore pressure, and temperature remain constant throughout the experiment, the displacement observed as a function of time is directly related to the shortening of the specimen. The LVDT measures the stretch of the vessel and the shortening of components in the sample assembly during initial loading. In order to separate the strain of the specimen from the deformation of the test apparatus, a series of test calibrations were conducted using a fused quartz specimen. Therefore, with the appropriate system corrections, the total strain of the specimen versus time can be calculated. This procedure is discussed under "System Calibration."

Radial strain was not measured on these specimens. Conventional instrumentation operates satisfactorily to temperatures of 150 °C. Such devices include strain gages, strain gage based transducers, and LVDTs. In some cases, the limit can be extended up to temperatures in excess of 200 °C. Alternatively, a dilatometric technique may be employed using a servo-controlled intensifier for tests conducted at constant confining pressure. As the volume of the specimen increases, fluid is expelled from the vessel, and the piston in the intensifier retracts. By monitoring the retraction of the piston, the volume change of the

specimen is obtained. If the axial strain is measured independently, the radial strain can be computed.

For this suite of creep measurements, the piston diameter on the output side of the confining pressure intensifier is 82.5 mm. To resolve a volumetric strain of 2.5×10^{-5} , we need to measure piston displacements of 9.3×10^{-5} mm. Displacement transducers under ambient conditions easily resolve the required displacements. However, the friction of the seals in the intensifier, temperature fluctuations in the laboratory, and small leaks in the system tend to overwhelm the resolution of the measurements with such a large bore intensifier. For these reasons, radial strain was not measured for these creep experiments.

One experiment was conducted in the conventional four post deformation apparatus described previously by Martin et al., (1991). The test was performed using the same experimental set-up and sample geometry described previously. However, a smaller pressure vessel (bore diameter = 101.8 mm) and external heating are utilized. The entire vessel is externally heated using the same method described above. Specifically, three band heaters are positioned on the outside of the pressure vessel to obtain the optimum thermal gradient along the axis of the specimen. The furnace assembly is encased with 40 mm thick fiber insulation and protected with a stainless steel cover. The axial strain of the specimen is accomplished with internal LVDTs mounted directly on the sample as reported previously.

2.3.2 System Calibration

System calibration consists of two procedures to verify suitable operation of the test apparatus in accordance with the ASTM procedure for creep. First, the temperature gradient along the length of the sample can deviate from end to end by no more than ± 3 °C. Furthermore, the variation in temperature at the midpoint of the sample for the duration of the test must be within ± 1 °C. Second, the deformation of the test system

components must be determined in order to remove their effects from the measurements on tuff specimens.

2.3.2.1 Temperature Gradient in Tuff Specimens

In order to set up the system to achieve a nearly constant temperature throughout the tuff specimen, a dummy specimen of tuff with an axial hole is used to check the thermal performance of the system. The test specimen of tuff is jacketed in the same manner as the tuff to be tested in creep. The specimen is inserted in the pressure vessel and subjected to a confining pressure of 10 MPa. A small differential stress is applied to the specimen. The temperature is then increased to 225 °C . Once the system reaches thermal equilibrium, the temperature is profiled along the axis by moving a thermocouple stepwise along the sample column; access is through the pore pressure inlet (see Figure 3). A thermocouple outside of the specimen is used to measure the temperature at the mid point of the specimen. If the temperatures at the ends of the specimen differ from that at the mid point of the specimen by more than 3 °C the furnace configuration is unacceptable. The heating bands are adjusted and the specimen is profiled again. If the temperature profile is within specification, the furnace configuration is acceptable. An example of this procedure is shown in Figure 5. Two temperature profiles along the axis of a dummy test specimen are shown as a function of position within the test specimen. The solid squares indicate an initial configuration where the temperature is too low at one end of the specimen (80 - 100 mm). The furnace rings were then repositioned, and an acceptable temperature gradient is achieved (the data shown in diamonds). This procedure was repeated for each vessel used in the study.

2.3.2.2 Correction for Displacement of the Test System

Since the displacement measured in the creep experiments is external to the pressure

Creep Vessel #2 Temperature Profiles

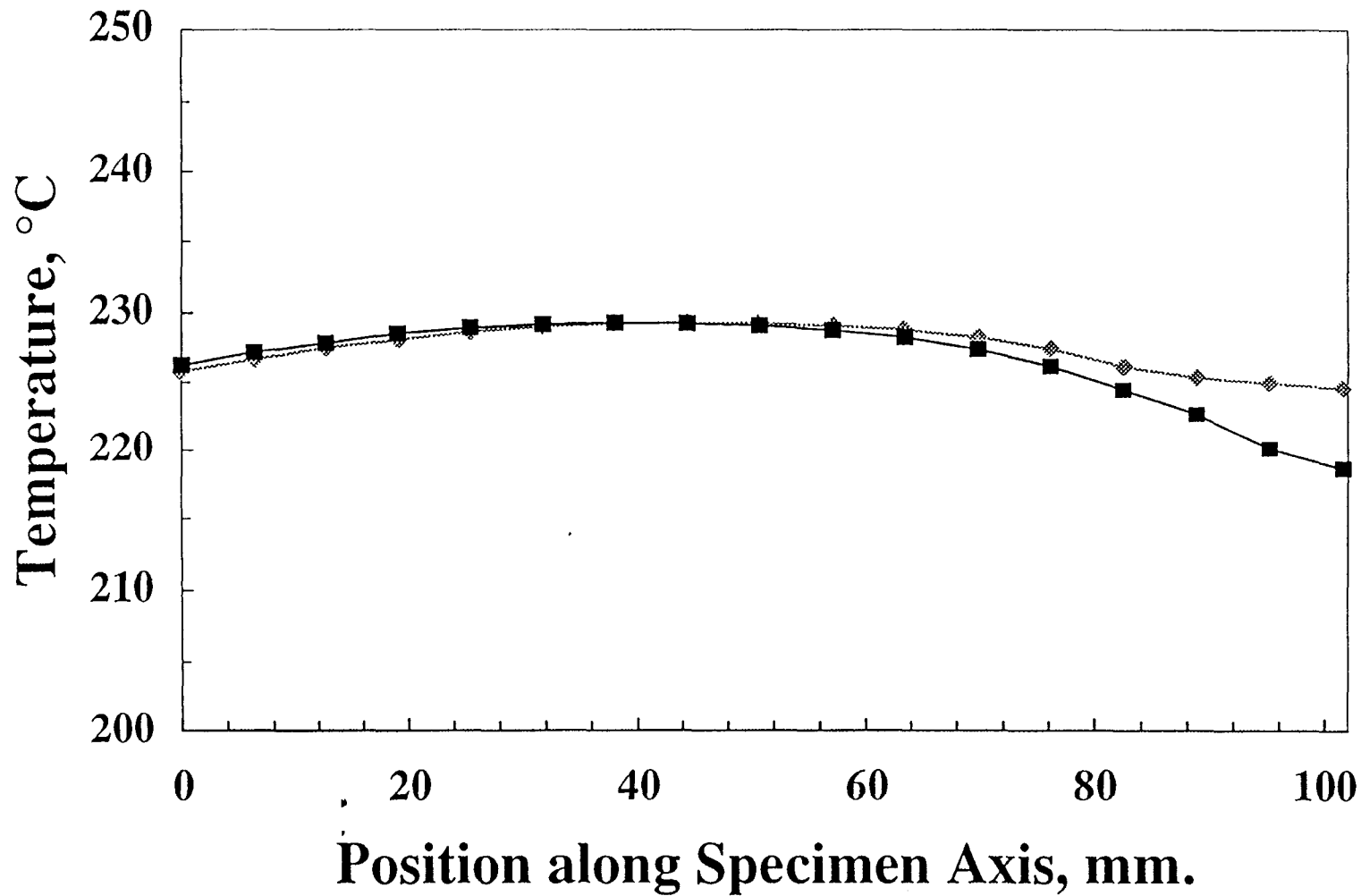


Figure 5: Temperature profile along the axis of a tuff specimen measured in creep vessel #2. The squares indicate initial profile with a large temperature gradient across the specimen. The diamonds indicate a satisfactory temperature profile resulting from repositioning furnace elements.

vessel, the total deformation of the sample column as well as stretching of the vessel are measured. The goal is to separate the shortening of the tuff specimen from the total displacement. The assumption is that the components of the system will experience elastic deformation during loading and all subsequent changes (time dependent deformation) are attributable to the shortening in the tuff specimen. Each test system is calibrated using a specimen of fused quartz. A confining pressure of 10 MPa is exerted on the specimen, and the temperature of the system is increased to 225 °C. The system is then monotonically loaded to a differential axial stress in excess of 100 MPa. The shortening of the sample column and stretch of the vessel are measured with the external displacement transducer (LVDT). The moduli of fused quartz are well documented. The displacement attributable to the quartz is subtracted from the total displacement. This difference is the system correction as a function of stress difference. The correction is applied to data collected in a creep experiment to obtain the axial strain of the test specimen.

An example of the results of the system calibration procedure is shown in Figure 6. A fused quartz specimen is placed in the vessel. A confining pressure of 10 MPa and a temperature of 225 °C is exerted on the specimen. The stress difference on the specimen is then increased to 100 MPa. Axial displacement is plotted as a function of stress difference in Figure 6. A total displacement of 0.32 mm is observed at a differential stress of 100 MPa. The calculated displacement attributable to fused quartz is also shown. The quartz displacement is slightly greater than 1/3 of the total observed displacement. The difference between the total displacement and the fused quartz displacement at each pressure represents the system correction that was applied to the data collected on tuff to obtain the specimen displacement. The system corrections for each of the three vessels are very similar; these data are shown in Figure 7.

The strain resolution using an external LVDT to monitor specimen shortening is at best 4×10^{-6} for this test configuration. However, considering external influences such as

Creep Vessel #2 - System Calibration Confining Pressure: 10 MPa; Temperature: 225 °C

18

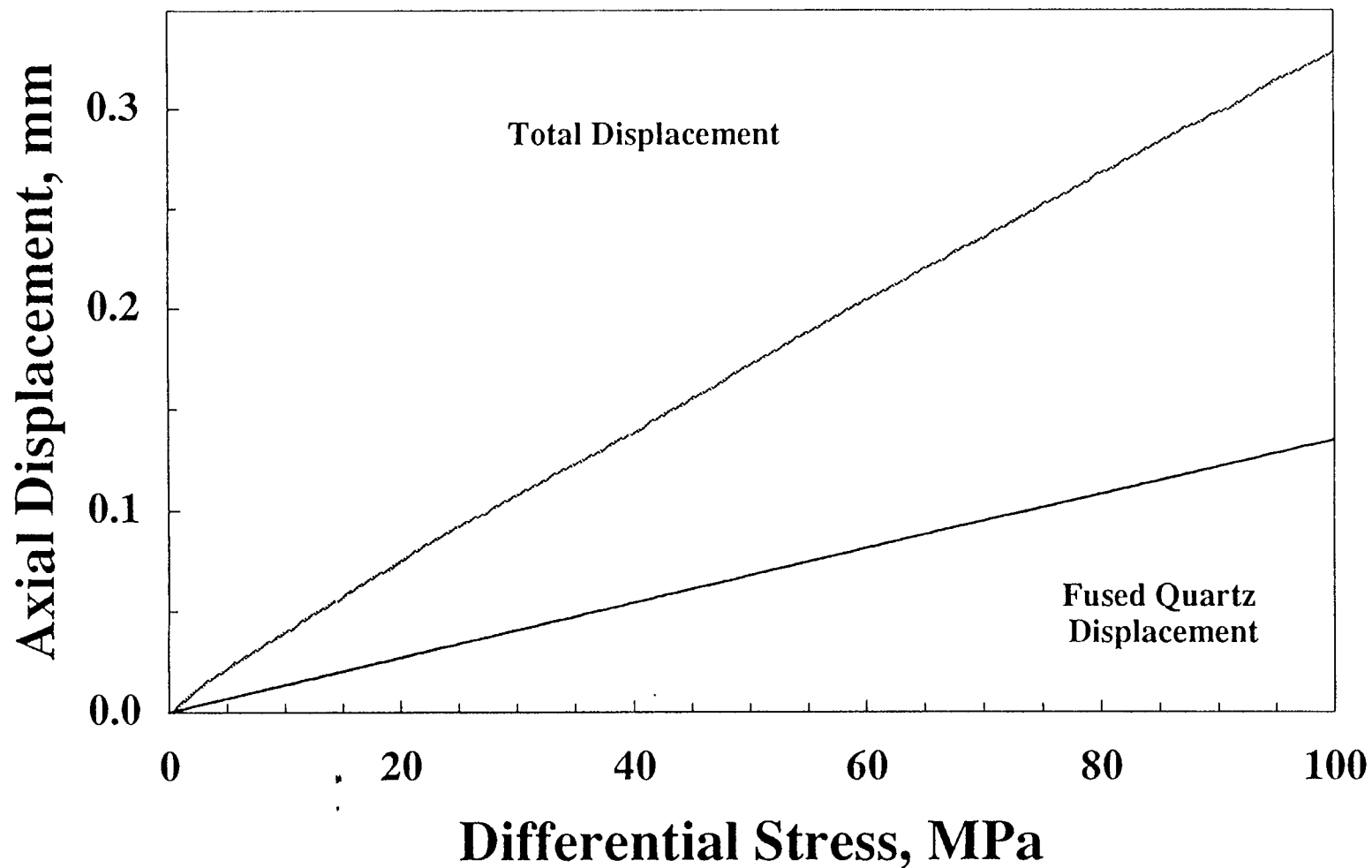


Figure 6: Displacement as plotted as a function of differential stress for a fused quartz specimen loaded in creep vessel #2. The computed displacement for a 101.8 mm long specimen of fused quartz is plotted for reference.

System Corrections

Confining Pressure: 10 MPa; Temperature: 225 °C

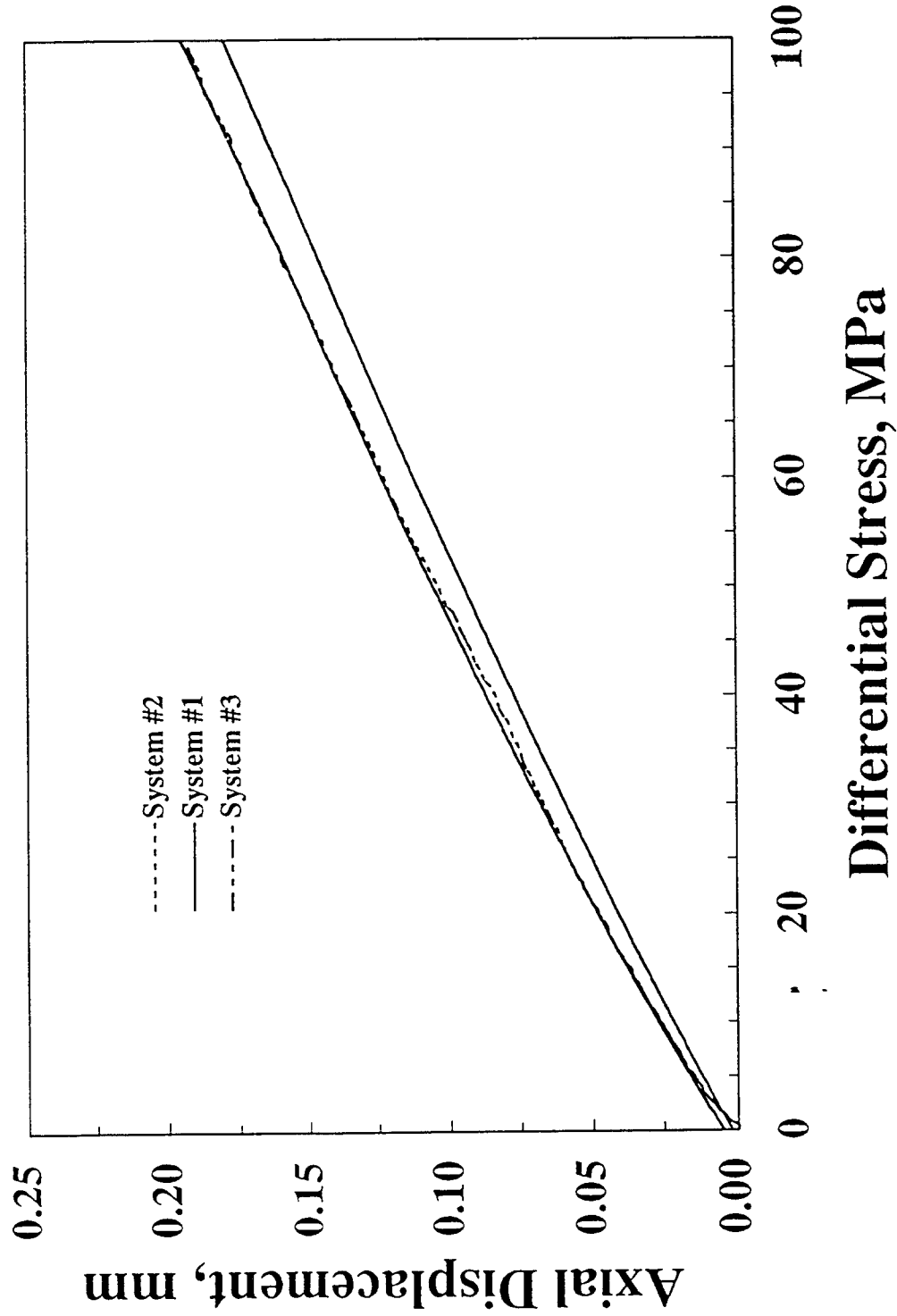


Figure 7: The system corrections for each creep apparatus are shown. Axial displacement is plotted as a function of stress difference. These corrections are used to obtain the strain in tuff specimens from the total system response in creep measurements.



ambient temperature changes, cultural disturbances in the laboratory, thermal drift in the electronics and the transducer, and seal friction effects, the practical resolution of strain is 1.2×10^{-5} .

2.3.3 Experimental Procedure for Creep Experiments at Elevated Temperature and Pressure

Seven specimens of tuff were tested at constant differential stress, confining pressure, and temperature for a minimum duration of 2×10^6 seconds. The following section includes the step-by-step procedures used to conduct the experiments. All seven of the experiments were performed at a confining pressure of 10 MPa and a temperature of 225 °C. The test procedure relies on ASTM D 4406-93, “Standard Test Method for Creep of Cylindrical Rock Core Specimens in Triaxial Compression.”

1. Machine each test specimen according to SNL TP-51. Measure ultrasonic velocities of each specimen after the machining process is complete.
2. List all transducers used in each experiment. The information includes the serial number of the device, signal conditioning amplifier number, the computer channel on which the output is recorded, and the scaling factor of the amplified output.
3. Visually inspect the specimen and note any surface irregularities and imperfections.
4. Jacket the specimen. The jacket consists of two layers of 0.13 mm thick dead soft copper wrapped around the specimen and extending 12 mm beyond the end of each specimen. Hardened steel end caps are then positioned at the end of the test specimens. The entire sample assembly is then jacketed with teflon heat shrink tubing and secured with two wraps of

wire at each end.

5. Insert the sample assembly into the pressure vessel.
6. Advance the loading piston until a small force is exerted on the specimen column.
7. Increase the confining pressure to 10 MPa.
8. Increase the temperature of the specimen to 225 °C at a rate no greater than 2 °C per minute.
9. Allow the system to reach thermal equilibrium for at least three (3) hours.
10. With the loading piston in contact with the specimen at a nominally zero differential stress, make the final mechanical adjustments on the external displacement transducer (LVDT).
11. Initiate data acquisition. The amplified outputs from four transducers are monitored and recorded using a micro-processor based data acquisition system. The transducers that are monitored include the LVDT, a thermocouple at the midpoint of the test specimen, and two pressure transducers measuring the axial pressure and the confining pressure. All channels are sampled every 0.25 seconds. Data is stored when the output of one channel deviates from the previous by a preselected threshold. The threshold for data acquisition is set prior to the experiment.
12. The differential stress on the sample assembly is rapidly increased to its preselected value. This is accomplished by briefly closing the valve to the high pressure side of the test chamber. The pressure is then increased to the

calculated value required to exert the specified differential stress. The valve is then opened to load the specimen. Loading of the specimen using this technique is accomplished in less than ten seconds.

13. The output of each of the transducers is monitored continuously until the sample fails or the experiment is terminated.

14. Remove the specimen from the test chamber and examine any features related to deformation failure of the specimen. Record the observations in the Scientific Notebook.

15. Return the specimen to its original container and return it to storage.

16. Reduce the data. The following information is determined: axial strain of the specimen, (which is equal to the change in length of the specimen, corrected by the system strain, divided by its total length), temperature, confining pressure, and differential axial stress. Each of these parameters are plotted as a function of time.

2.3.4 Test Performed in Large Load Frame

One experiment was conducted in a conventional four post test apparatus. The characteristics of this test system have been reported previously (Martin et al., 1991). The creep experiments were conducted according to the procedures established in the earlier study. The only difference in procedure between the system described above and this system is that the axial force on the specimen was computed using an external load cell and the deformation of the specimen was measured with LVDT's mounted directly on the endcaps of the specimen. Corrections were made for the deformation of the end caps in computing the total strain of the specimen.

3.0 RESULTS

The results of the creep measurements on the TSw2 welded tuffs are presented in Table 1, and Figures 8 through 19. Experiments were conducted at nominal differential stresses of 40, 70, 100, and 130 MPa at a confining pressure of 10 MPa and a temperature of 225 °C. The specimens were tested drained.

The test on specimen NRG-7-808.3 was conducted in the four post test frame at a differential stress of 130 MPa. The experiment was terminated prior to failure after 5.9×10^6 seconds. Figure 8 shows axial strain as a function of time. The strain change is extremely small. The elastic deformation during initial loading is near 3.01×10^{-3} . Little additional strain accumulated during the experiment. In fact, at the termination of the test the strain on the specimen was less than 3.06×10^{-3} .

Figure 9 gives the stress difference exerted on the specimen as a function of time. The stress on the specimen remained constant to better than ± 0.25 MPa for most of the experiment. There was one deviation as the duration of the experiment approached one million seconds. The fail-safe on the test system was activated due to a broken electrical lead. The solenoid valves locked the hydraulic cylinder that exerts the axial load; this resulted in a decrease in the axial force on the system. The lead was repaired and the solenoid valves opened. The differential stress on the specimen returned to 130 MPa. The stress remained constant for the remainder of the experiment. The interruption in loading also caused a corresponding change in the axial strain. When the specimen was reloaded, the specimen achieved the same axial strain level as prior to the decrease in stress.

Figure 10 shows the temperature as a function of time. The temperature varies by ± 2.5 °C. Although this exceeds the ASTM recommendation of ± 1.0 °C, the effect on the strain is small.

Table 1

SUMMARY DATA SHEET: USW NRG-7/7A BOREHOLE

Creep Tests

Sample IDs are shortened from the "NRG-7/7A-Depth-SNL-Subdivision" Format
 Nominal Sample Dimensions: Length = 101.60 mm; Diameter = 50.80 mm

24

Depth, ft:	776.6	807.6	808.3	858.4	1264.5	1281.4	1400.5
T/M Unit:	TSw2						
Lithostratigraphic Unit:	Tptpmn	Tptpmn	Tptpmn	Tptpmn	Tptpln	Tptpln	Tptpln
Date Test Initiated:	3/28/95	3/28/95	2/17/95	3/28/95	9/30/93	9/30/93	9/30/93
As Tested Bulk Density (g/cc):	2.249	2.273	2.295	2.307	2.295	2.295	2.295
Average Grain Density (g/cc):	2.536	2.534	2.526	2.526	2.591	2.592	2.515
Porosity (%)	11.3	10.3	9.2	8.7	11.4	11.5	8.8
P Velocity (km/s):	4.357	4.426	4.455	4.488	4.064	4.431	N/A
S1 Velocity (km/s):	2.774	2.775	2.800	2.816	2.563	N/A	N/A
S2 Velocity (km/s):	2.730	2.712	2.848	2.769	2.510	N/A	N/A
Radial P Velocity (km/s):	4.388	4.418	4.471	4.465	4.450	4.618	N/A
Radial S Velocity (km/s):	2.808	2.836	2.824	2.847	2.703	2.815	N/A
Temperature, °C	225	225	225	225	225	225	225
Confining Pressure, MPa	10	10	10	10	10	10	10
Stress Difference, MPa	70	40	129	100	98	132	131
Strain @ 1,000s (millistrain)	2.34	1.08	3.02	2.69	3.01	3.70	3.47
Strain @ termination (millistrain)	2.52	1.16	3.06	2.88	3.25	4.04	3.84
Duration of Test Days	43.5	43.5	68.3	43.5	29.5	29.5	29.5
Duration of Test (millions of seconds)	3.76	3.76	5.90	3.76	2.55	2.55	2.55

P is the compressional wave; S1 and S2 are the two orthogonally polarized shear waves.

Topopah Spring Member Tuff, TSw2

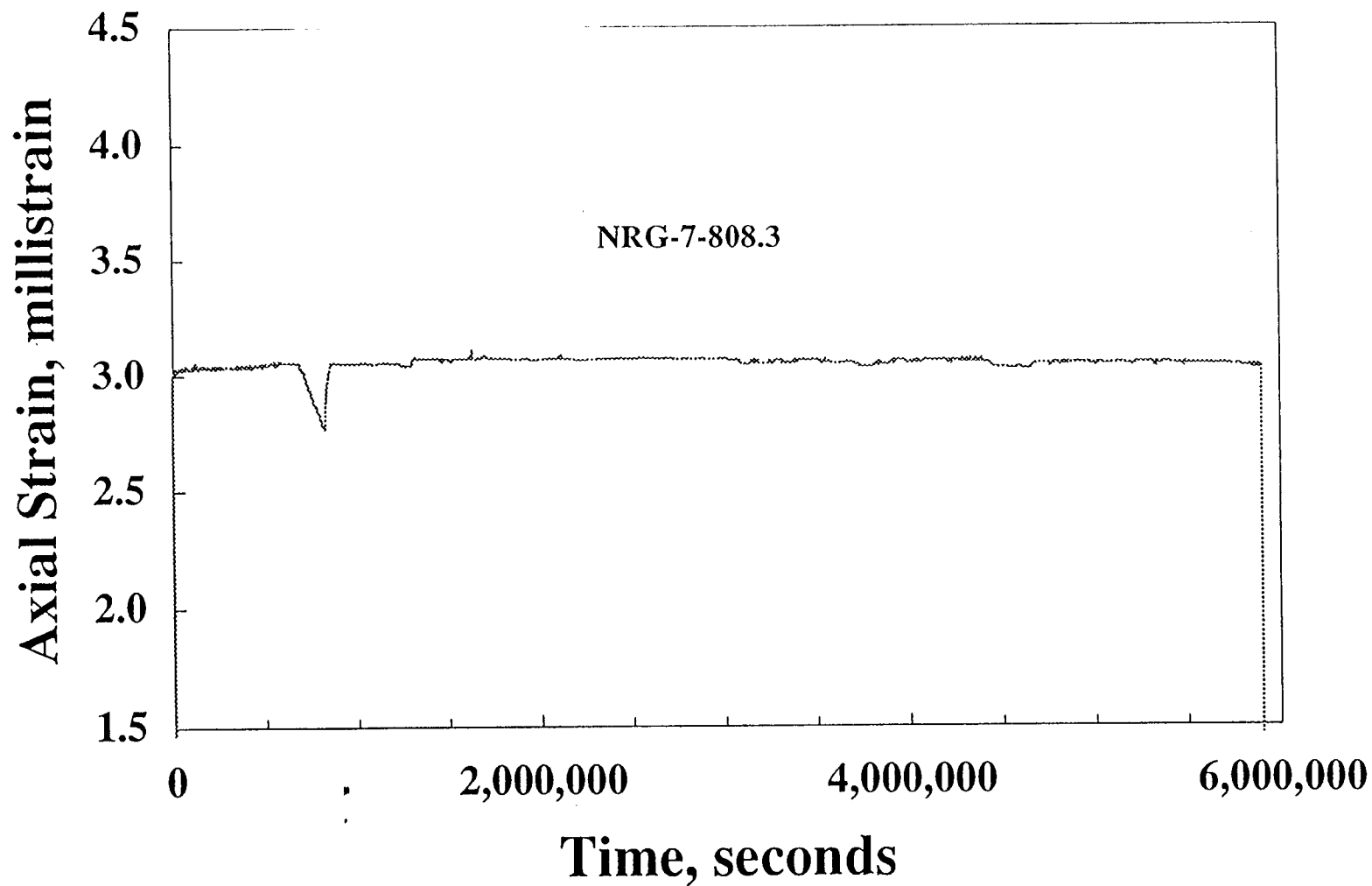


Figure 8: Axial strain is plotted as a function of time for a creep test at 225 °C at a confining pressure of 10 MPa for welded tuff specimen (NRG-7-803).

Topopah Spring Member Tuff, TSw2

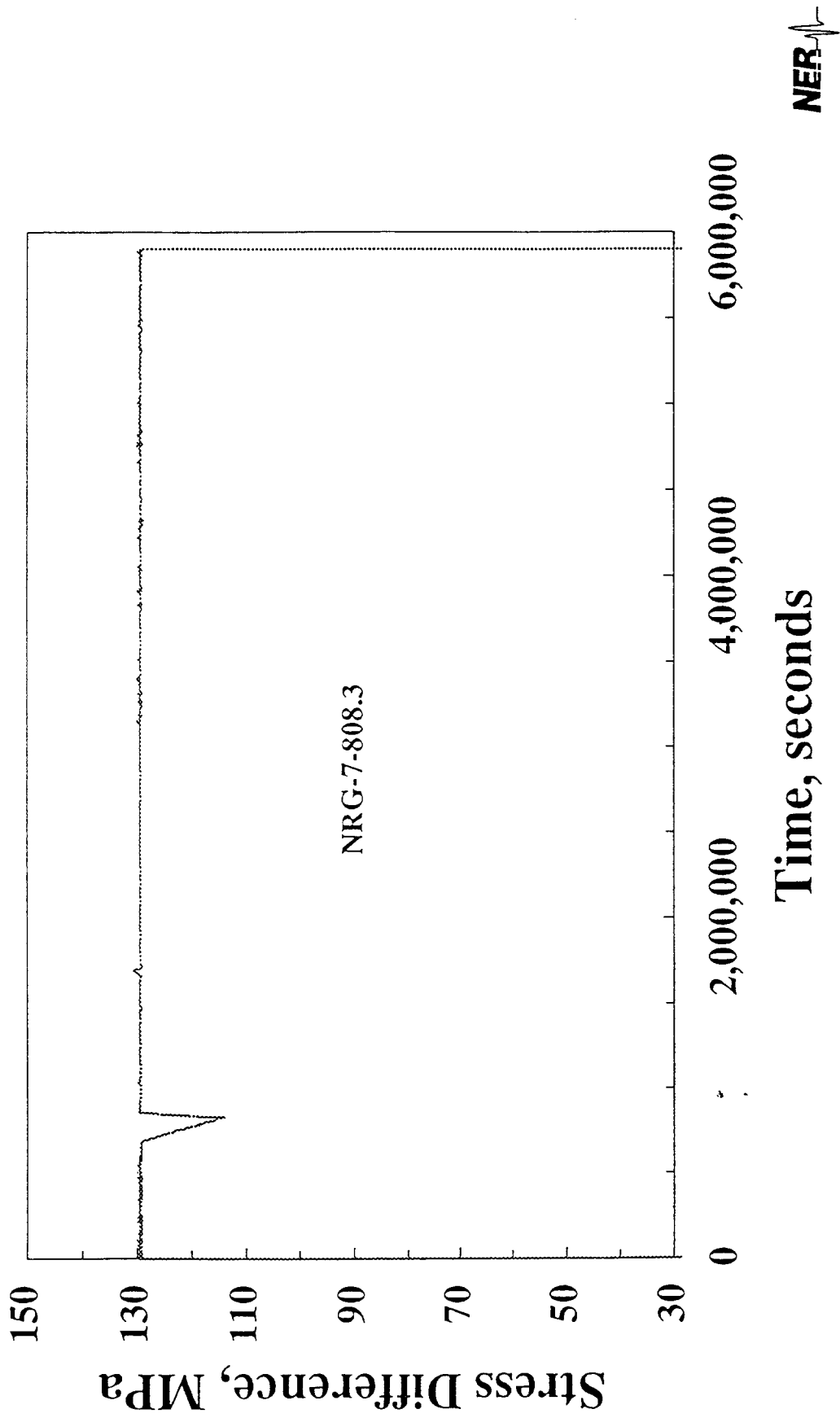


Figure 9: Stress differences plotted as a function of time for a creep test conducted at 225 °C at a confining pressure of 10 MPa for specimen NRG-7-808.3.

Topopah Spring Member Tuff, TSw2

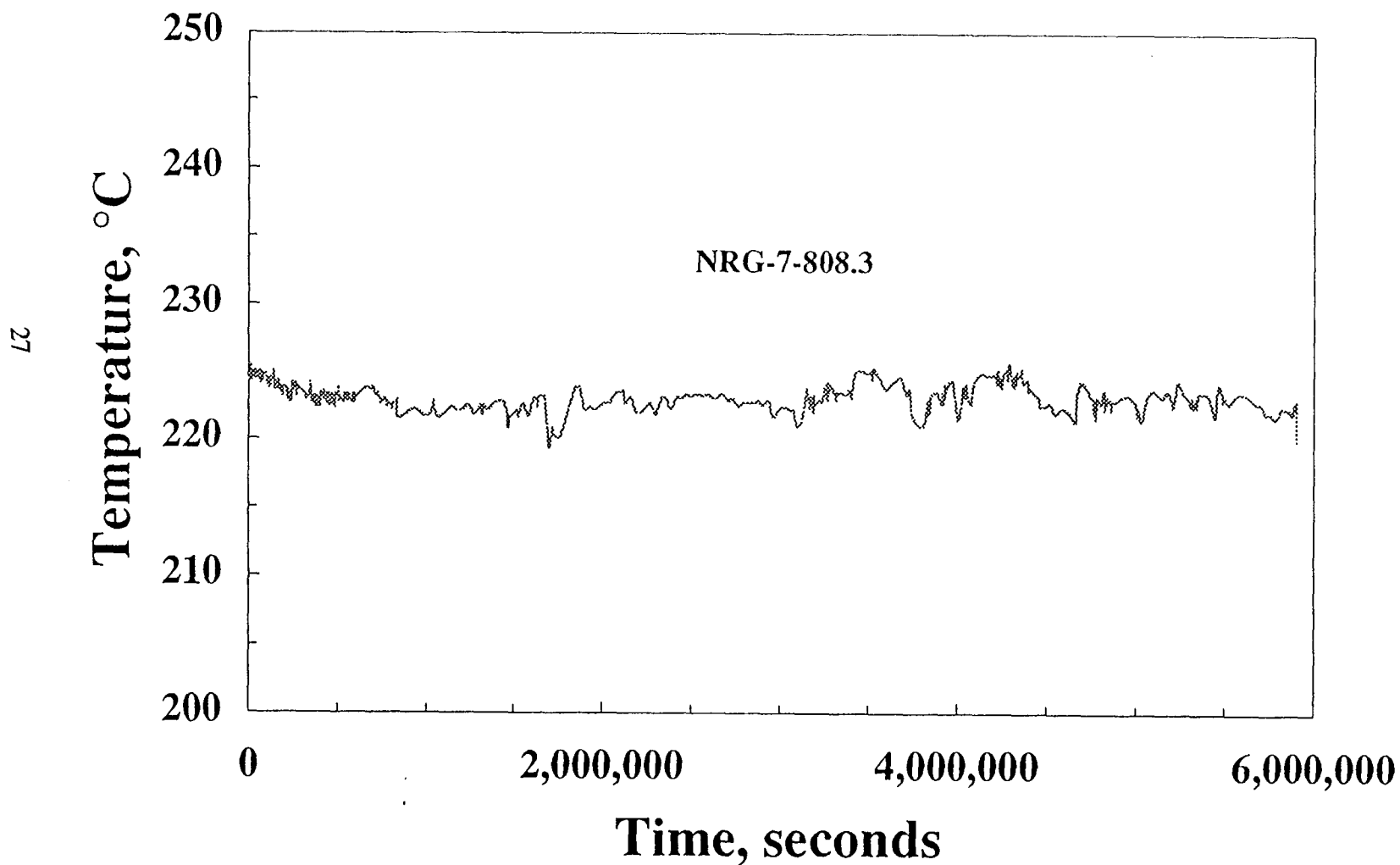


Figure 10: Temperature at the mid-point of a specimen plotted as a function of time for a creep experiment at a differential stress of 130 MPa and a confining pressure of 10 MPa on a welded tuff specimen (NRG-7-808.3).

Specimens NRG-7-776.6, 807.6, and 858.4 were tested simultaneously at differential axial stresses of 70, 40, and 100 MPa respectively. The axial strain data obtained for these experiments are shown in Figure 11. Axial strain is plotted as a function of time. Specimen NRG-7-807.6 with a differential stress of 40 MPa, developed a strain of nearly 1.1×10^{-3} during loading. No additional strain accumulation was detected. An O-ring on the loading piston failed at near 1.5×10^6 seconds into the test. The temperature and confining pressure were decreased. The O-ring on the piston was repaired and the sample was reloaded. On reloading the specimen exhibited nearly the same strain as prior to the O-ring failure. No additional strain accumulation was noted for the duration of the test.

Specimen NRG-7-776.6 was tested at a differential axial stress of 70 MPa. Initial loading produced a strain of 2.42×10^{-3} . The specimen continued to shorten throughout the test. The strain rate was not constant; it continually decreased with time. The strain began to decrease at approximately 3.7×10^6 due to a jacket failure; the test was terminated.

Specimen NRG-7-858.4 was tested at a differential axial stress of 100 MPa. Initial loading produced an axial strain in excess of 2.7×10^{-3} . Strain accumulation continued throughout the experiment. The rate of strain accumulation was not constant. The strain rate was greatest in the first 1×10^6 seconds. Subsequently, the strain accumulation decreased to a low rate.

The stress difference and temperature for these experiments are plotted as a function of time in Figures 12 and 13. The data indicate that the stress is constant and well defined for each experiment. The temperature at the midpoint of the specimens varies by ± 1.0 °C. No discernible effect of the fluctuation is observed in the strain. All three experiments were terminated simultaneously at 3.7×10^6 seconds. NRG-7-776.6, NRG-7-807.6 and NRG-7-858.4 were intact. No evidence of visible damage to the three specimens was

Topopah Spring Member Tuff, TSw2

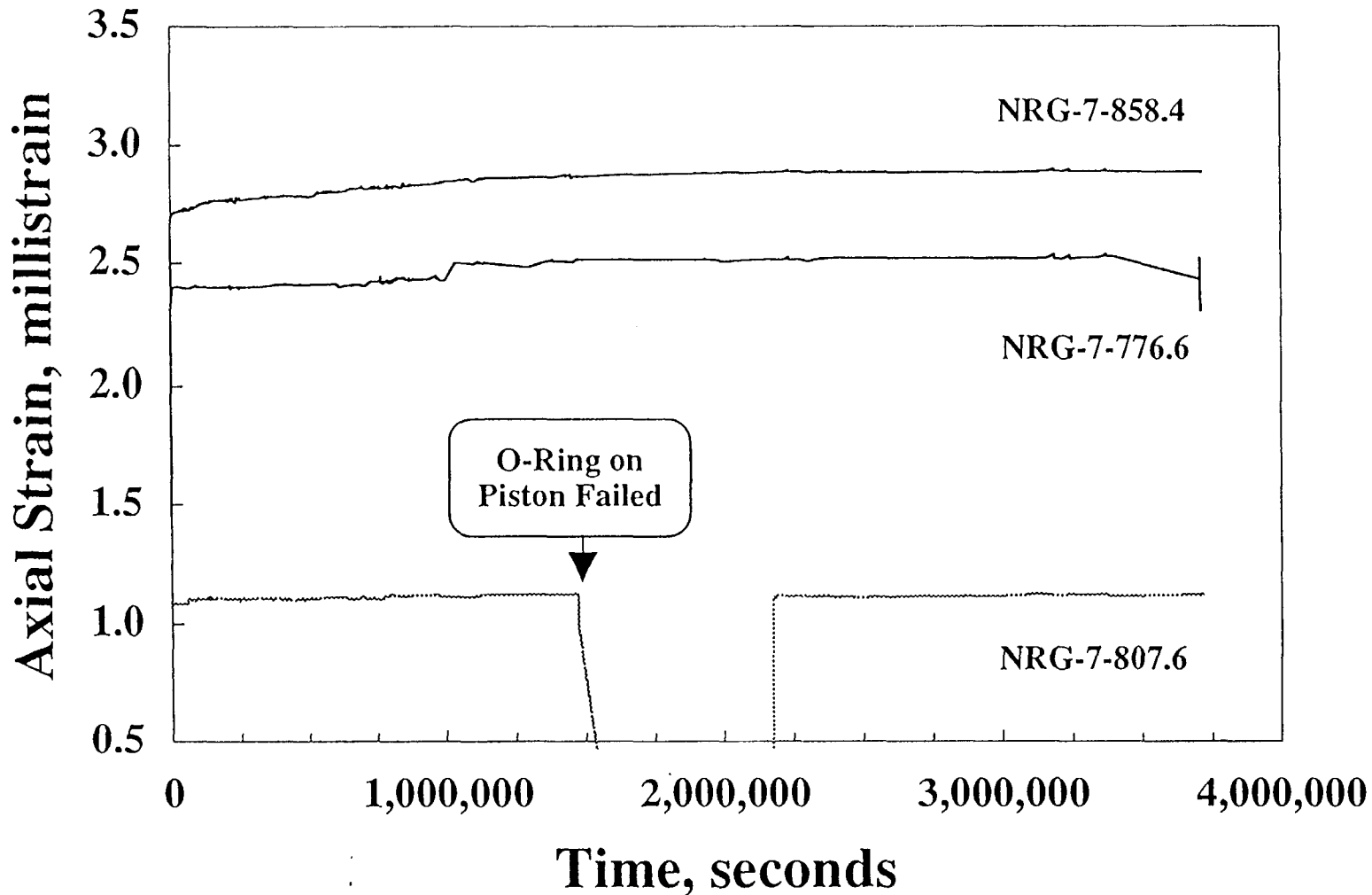


Figure 11: Axial strain plotted as a function of time for three creep experiments conducted simultaneously in independent test systems. All of three experiments were conducted at a confining pressure of 10 MPa and a temperature of 225 °C. NRG-7-858.4 was conducted at a differential stress of 100 MPa; NRG-7-776.6 was conducted at a differential stress of 70 MPa; and NRG-7-807.6 was conducted at a differential stress of 40 MPa.

Topopah Spring Member Tuff, TSw2

30

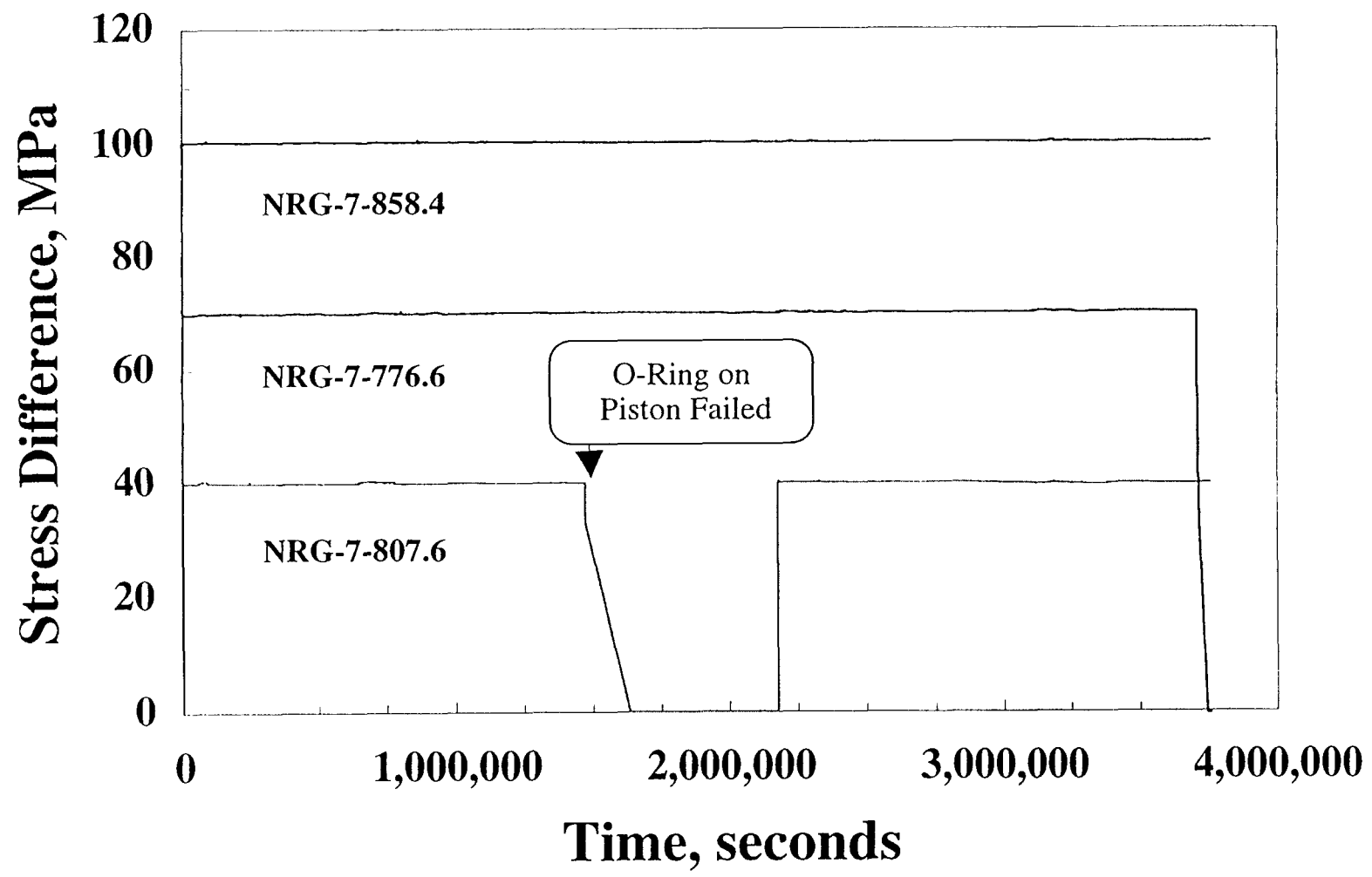


Figure 12: Stress differences is plotted as a function of time for three creep experiments tested simultaneously in independent systems. The experiments were conducted at a confining pressure of 10 MPa and a temperature of 225 °C.



Topopah Spring Member Tuff, TSw2

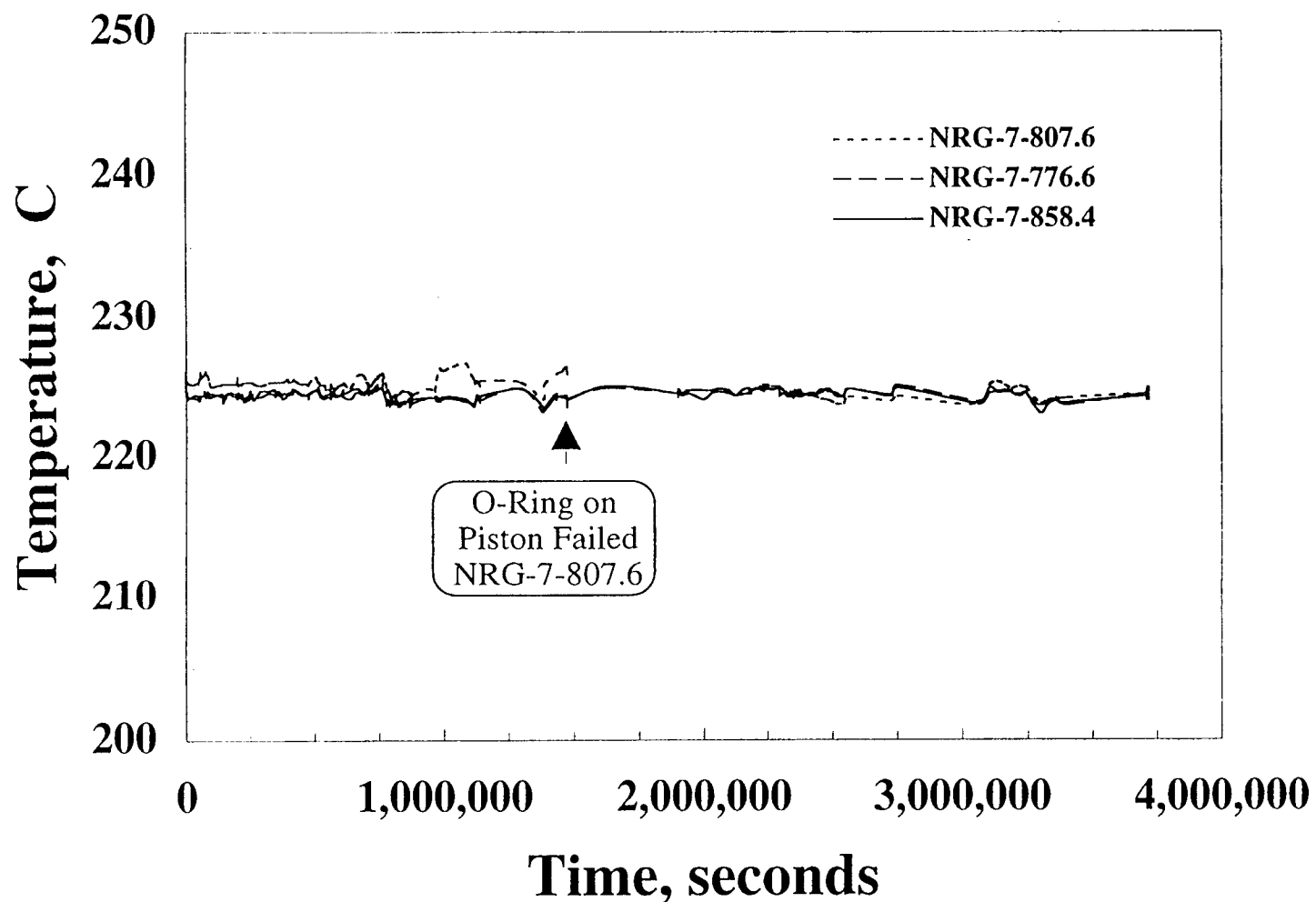


Figure 13: Temperature is plotted as a function of time for three experiments conducted simultaneously in independent test systems. Each experiment was conducted at a confining pressure of 10 MPa. Specimen NRG-7-858.4 was conducted at a stress difference of 100 MPa; NRG-7-776.6 was conducted at a stress difference of 70 MPa; and NRG-7-807.6 was conducted at a stress difference of 40 MPa.

detected.

Another suite of experiments was conducted on specimens NRG-7-1264.5, NRG-7-1281.4, and NRG-7-1400.5, at differential axial stresses of 98, 131, and 132 MPa respectively. The strains measured on these specimens are shown as a function of time in Figure 14.

Specimen NRG-7-1264.5 shows a significant transient strain upon initial loading. The inelastic strain change was greatest in the first several thousand seconds. As with the previous tests, the strain rate noted during secondary creep is not constant. After the specimen is subjected to stress for approximately 1×10^6 seconds, the strain rate decreases markedly. At approximately 2.57×10^6 seconds the jacket on the specimen failed and the experiment was terminated. An examination of the specimen showed no apparent damage to the specimen.

Specimens NRG-7-1281.4 and NRG-7-1400.5 were tested at a nominal stress difference of 130 MPa. The behavior of both samples is very similar. Both show significant transient strain at times less than one thousand seconds. The strain rate is not constant. Strain accumulates throughout the experiment, but the rate decreases with time.

The strain appears episodic in these two experiments. This is due to friction of the piston seal and friction between the LVDT core and barrel. A nonphysical event is noted for specimen NRG-7-1281.4 between 22,000 and 30,000 seconds. The strain apparently increases by 8.5×10^{-5} , remains constant for 8×10^3 s, and then decreases by 3.5×10^{-5} . This is anomalous behavior in the LVDT is attributable to friction between the core and barrel. A net increase in strain occurs over the interval but the time history is not accurately portrayed.

On July 24, 1995 severe weather in the area caused a power outage that lasted several hours. Although the data acquisition system is on an uninterruptible power supply (UPS), the furnaces and hydraulic system are not. Consequently, the temperature and state

Topopah Spring Member Tuff, TSw2

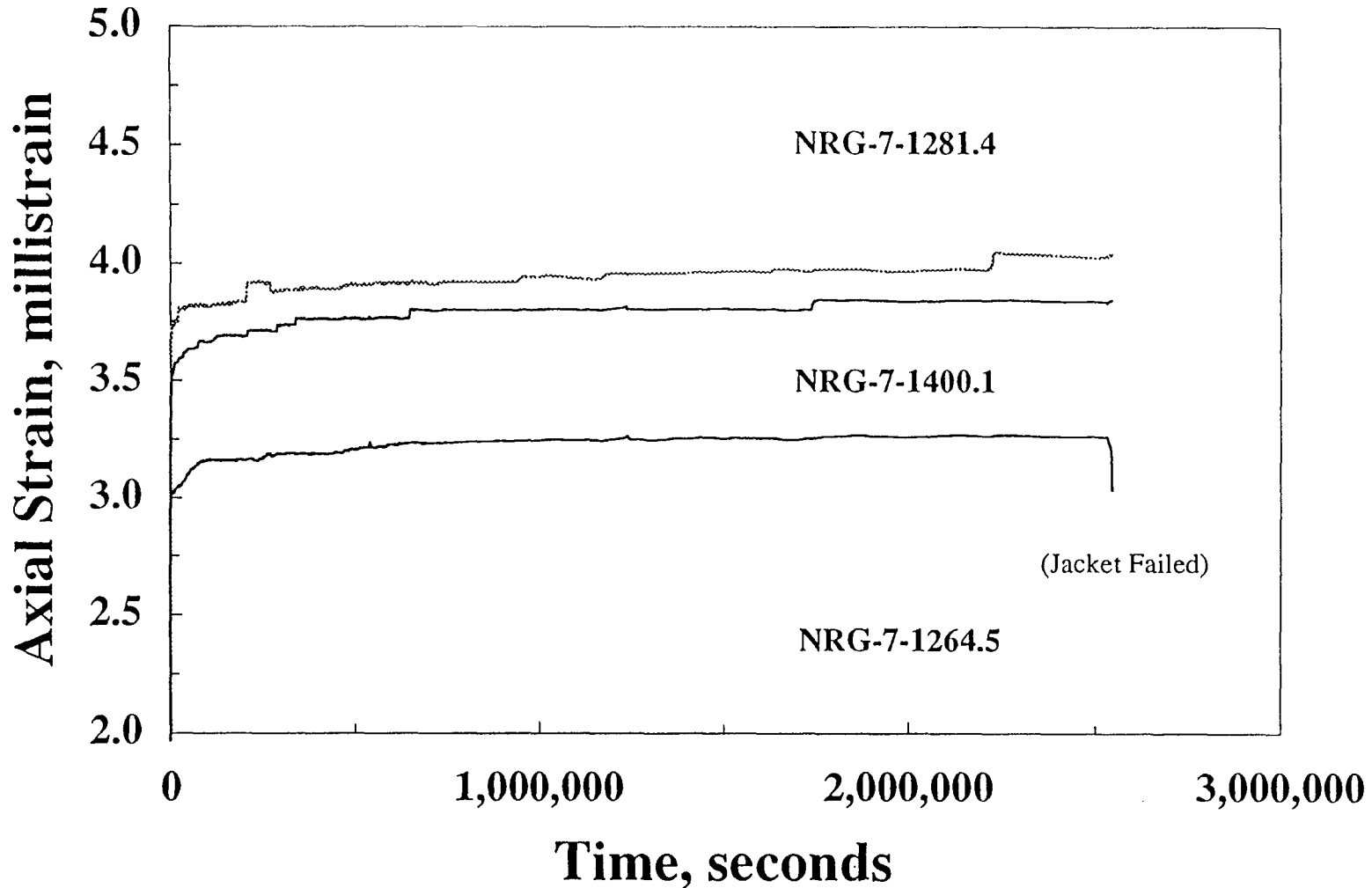


Figure 14: Axial strain plotted as a function of time for three creep experiments conducted simultaneously in independent test systems. All of three experiments were conducted at a confining pressure of 10 MPa and a temperature of 225 °C. NRG-7-1281.4 was conducted at a differential stress of 131 MPa; NRG-7-1400.5 was conducted at a differential stress of 132 MPa; and NRG-7-1264.5 was conducted at a differential stress of 98 MPa.

of stress of the specimens were not maintained. The experiments were terminated.

The stress difference and temperature for each of the specimens is plotted as a function of time in Figures 15 and 16 respectively. An examination of the data show that these parameters remain within specification throughout the experiments.

Specimens NRG-7-1264.5 and NRG-7-1400.5 showed no external indication of damage. A post-test examination of specimen NRG-7-1281.4 showed spall and cracking around a vapor-phase altered zone. This suggests that microcracking was occurring and that perhaps the fracture process was underway.

4.0 DISCUSSION

The data collected in the seven creep experiments show several consistent features. First, with increasing differential stress, time dependent strain increases. At 40 MPa, no perceptible time dependent strain accumulation is observed. However, with increasing differential stress to 70, 100 and subsequently 130 MPa, the rate of strain at constant stress increases. There is scatter in the results. For example, one experiment at a stress difference of 130 MPa shows no apparent strain accumulation even though the experiment lasted 5.9×10^6 seconds.

The data presented in Figures 8, 11 and 14 are replotted with a logarithmic time base in Figures 17, 18, and 19. A cursory examination of the data show that the strain accumulation is not linear with time; the strain rate is continually decreasing. These observations are consistent with models for creep in brittle silicate rocks based on stress corrosion cracking.

The strength of brittle rocks is dependent on the partial pressure of water surrounding the test specimen. For example, Charles (1959) observed that the compressive strength of nominally identical granite specimens tested in atmospheres of saturated steam and then dry nitrogen at a temperature of 240 °C increased by more than a factor of three.

Topopah Spring Member Tuff, TSw2

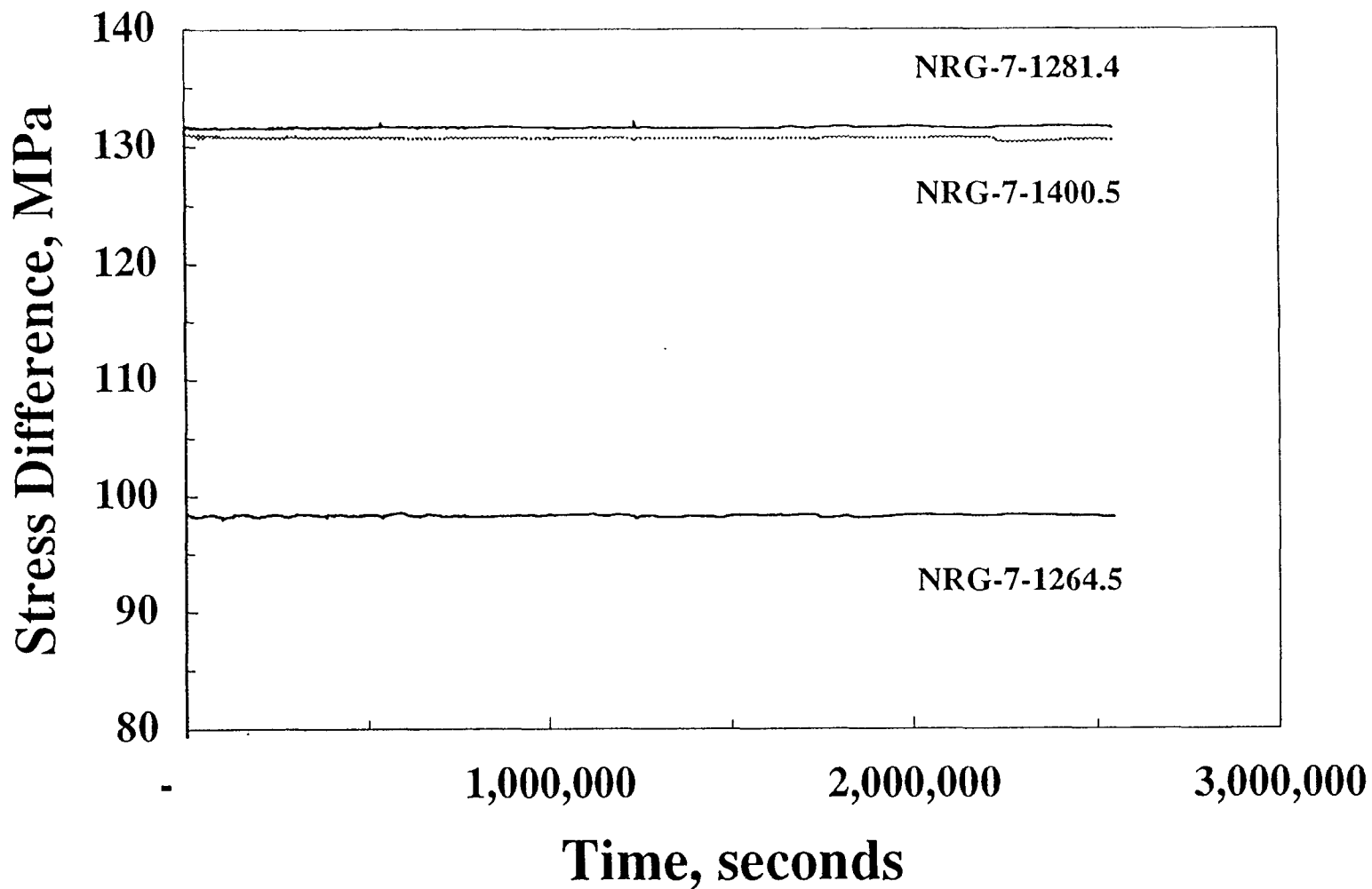


Figure 15. Stress difference is plotted as a function of time for three creep experiments conducted simultaneously in independent systems. The experiments were conducted at confining pressures of 10 MPa and a temperature of 225 °C.

Topopah Spring Member Tuff, TSw2

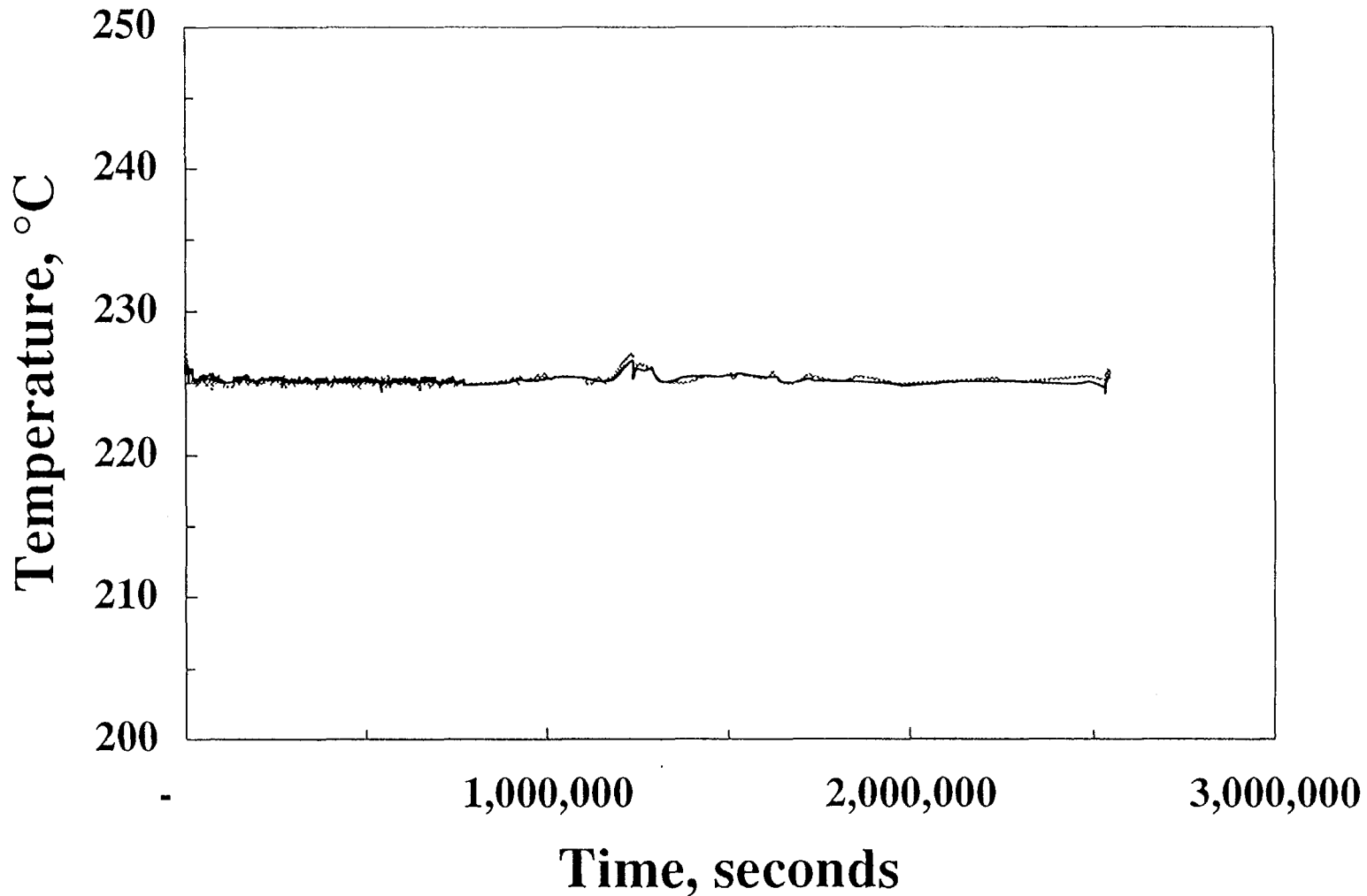
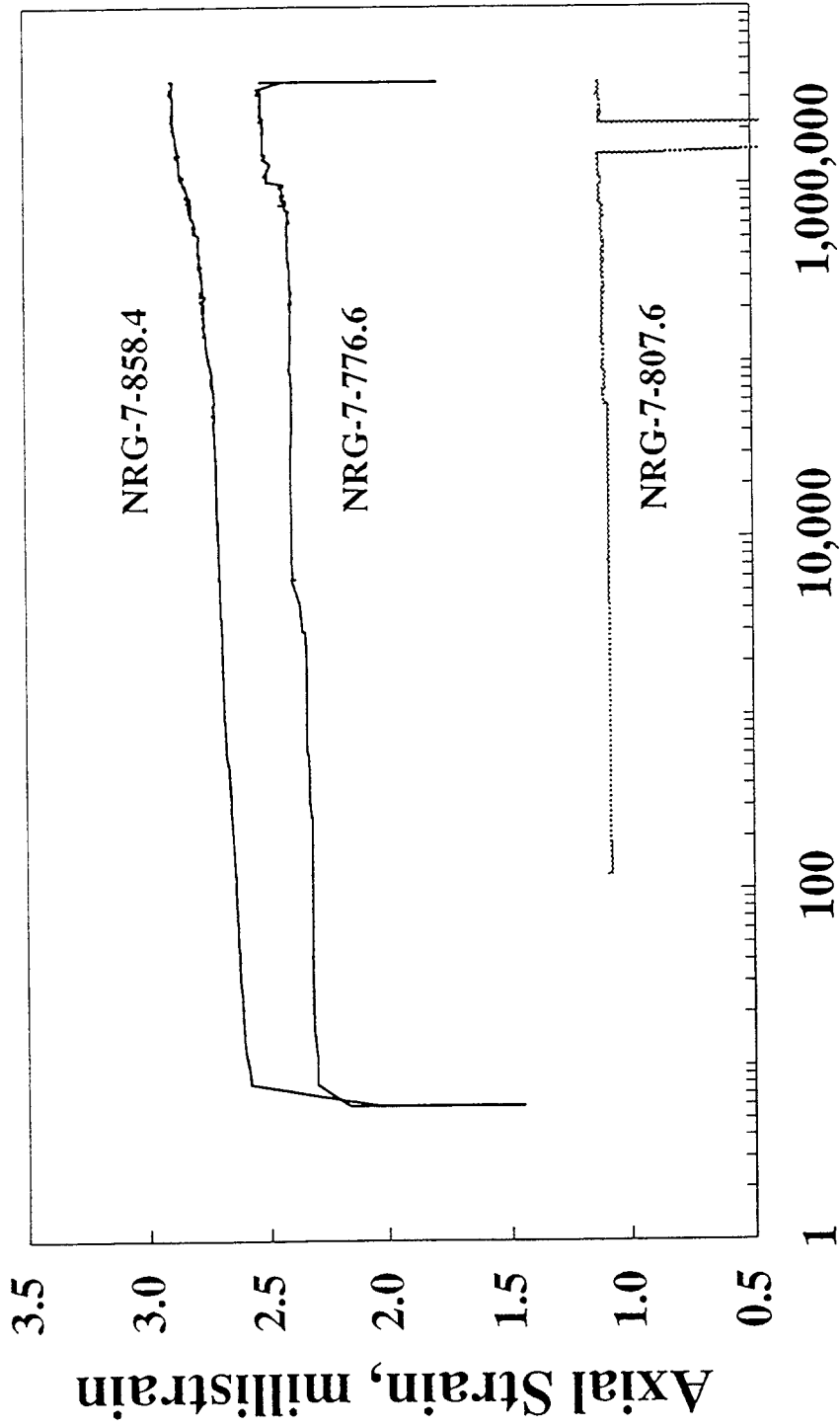


Figure 16: Temperatures are plotted as a function of time for three experiments conducted simultaneously in independent test systems. Each experiment was conducted at a confining pressure of 10 MPa. Specimen NRG-7-1281.4 was conducted at a stress difference of 132 MPa; NRG-7-1400.5 was conducted at a stress difference of 131 MPa; and NRG-7-1264.5 was conducted at a stress difference of 98 MPa.

Topopah Spring Member Tuff, TSw2



Time, seconds

Figure 17: Axial strain is plotted as the log time for specimens of welded tuff tested at a confining pressure of 10 MPa and a temperature of 225 °C. Specimen NRG-7-858.4 was conducted at a stress difference of 100 MPa; specimen NRG-7-776.6 was tested at a stress difference of 70 MPa; and specimen NRG-7-807.6 was conducted at a stress difference of 40 MPa.



Topopah Spring Member Tuff, TSw2

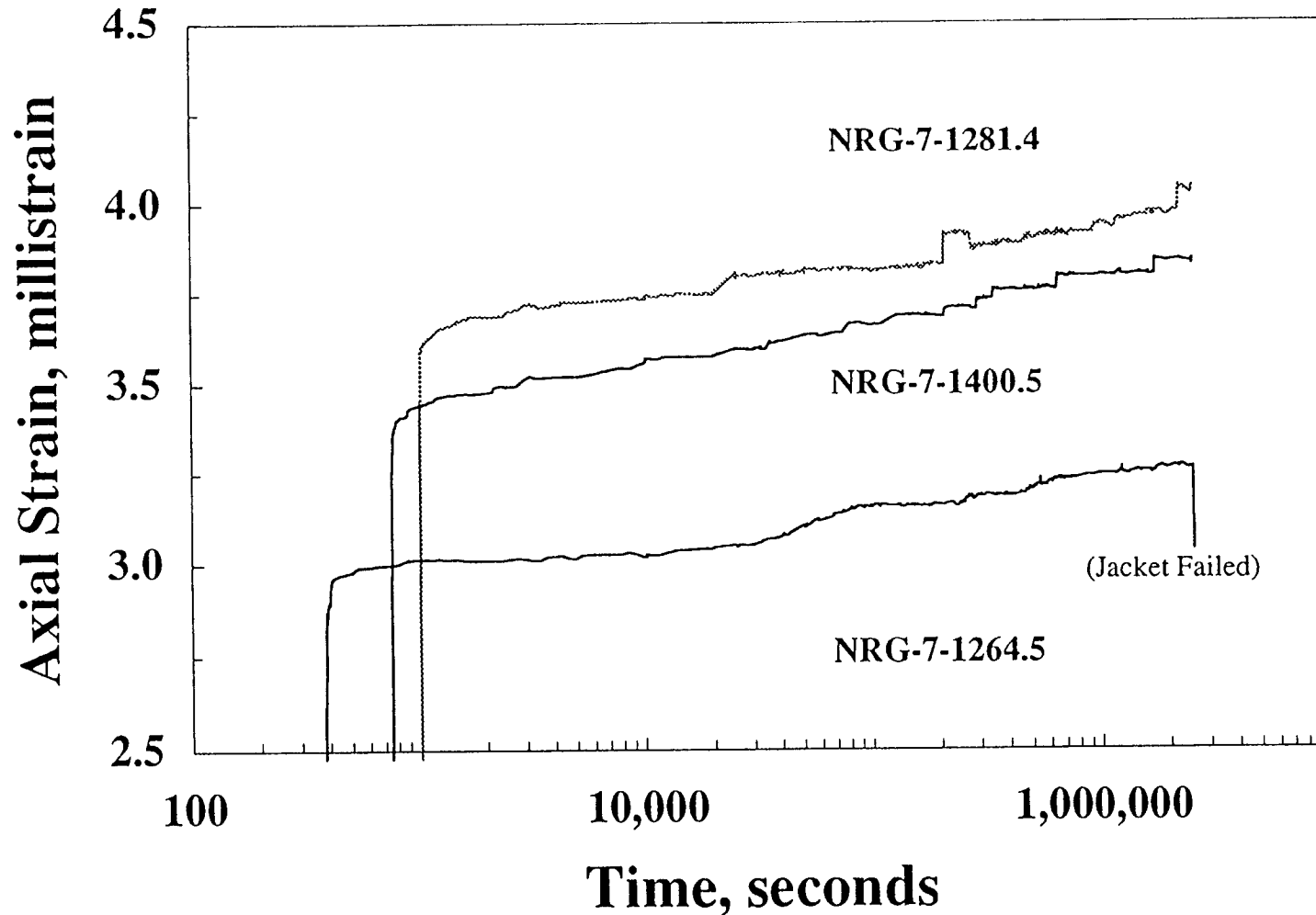


Figure 19: Axial strain is plotted as the log time for specimens of welded tuff tested at a confining pressure of 10 MPa and a temperature of 225 °C. Specimen NRG-7-1400.5 was conducted at a stress difference of 132 MPa; specimen NRG-7-1264.5 was tested at a stress difference of 70 MPa; and specimen NRG-7-807.6 was conducted at a stress difference of 100 MPa.

The mechanism of deformation and fracture in brittle silicates, including the tuff from the potential repository horizon, is characterized by the initiation and propagation of cracks parallel to the greatest compressive stress direction (see Brace et al., 1966). Studies of crack propagation have shown that the rate of crack propagation at a constant stress (stress intensity factor) and temperature is proportional to the partial pressure of water at the crack tip (see Wiederhorn, 1968). As the concentration of water (partial pressure of water) at the crack tip increases, the crack velocity increases; conversely, as the partial pressure of water decreases, the crack velocity decreases. Given that the mechanism of deformation and fracture in brittle rocks is the initiation and propagation of axial cracks and the strength is dependent on the water concentration surrounding the specimen, it is likely that the mechanism of creep is in some way related to moisture assisted crack growth (stress corrosion cracking).

Martin (1972), Martin and Durham (1975), and Dunning et al. (1980) studied crack growth in single crystals of quartz loaded in compression. For cracks propagating parallel to the loading axis at a fixed temperature, stress, and partial pressure of water, the rate of crack growth was not constant. The rate of crack propagation continually decreased with time. The change in crack length with time is best fitted by an expression of the form

$$C = At^n$$

where C is the crack length, t is time, and A and n are experimentally determined constants; n is always less than 1. The general form of the equation held for experiments conducted over a wide range of stress, temperature, and environmental conditions.

Crack growth experiments conducted in tension and the theory developed by Wiederhorn (1968) show that cracks grow at a constant velocity. This is not observed when the applied load is compressive. If the theory is correct, then the partial pressure of water at the crack tip must decrease with time. Several reasons have been forwarded to explain this behavior. First, the path length for water diffusion increases as the crack length

increases. Second, cracks lengthen when a hydration reaction alters strong Si-O bonds to form weaker Si-OH Van der Waal bonds which fail in local tension at the crack tip. There is a volume increase associated with the hydration reaction. The volume increase reduces the diffusivity along the crack. These effects result in a reduction in the rate that water is transported at the crack tip, which in turn inhibits the rate of growth. Third, the stress intensity factor at the crack tip decreases with increasing crack length.

Martin (1972) showed that for brittle rocks with randomly oriented cracks, creep is proportional to the rate of crack growth. If the only effect of increasing temperature, stress, or partial pressure of water is to augment the rate of crack growth on preexisting cracks, the same dependencies observed for isolated cracks in quartz will occur in brittle silicate rocks. The creep data for welded tuff exhibit the same form of time dependent behavior observed in single crystals of quartz and predicted by the model.

Brittle rocks differ significantly from rocks which undergo plastic deformation at low pressure and temperatures. For example, large strains are observed in rock salt at low differential stresses and moderate temperatures. In contrast, brittle rocks exhibit extremely small strains at failure even at temperatures in excess of 400 °C. The rheology for these rocks is different. Most notably, rocks exhibiting plasticity have a fairly well defined relationship between stress and the steady state strain rate at a fixed confining pressure and temperature. The creep strain for brittle rocks is small and the relationship between strain rate and stress is extremely difficult to determine even at high stresses. For rocks that exhibit plastic deformation, the objective is not to predict fracture but to estimate the total strain as a function of time for a given state of stress.

In brittle rocks, the strain at failure is extremely small (typically less than 0.5%) and varies by as much as a factor of two for nearly identical specimens. Furthermore, the creep strain accumulation is not linear with time. This makes estimation of the time to failure difficult to predict. For this reason, brittle rocks are often treated in terms of static fatigue.

That is, the time to failure is plotted as a function of the applied stress. In this way, an estimate of the long term strength of the rocks and a measure of its uncertainty can be achieved without specific reference to the associated strain.

The effect of water concentration (partial pressure of water) and temperature as well as the state of stress should be addressed in future experiments. The potential test matrix is extremely large. However, by conducting a number of critical tests to develop a relationship between time to failure, state of stress, temperature, and saturation, the number of tests can be limited (Martin et al., 1995).

Creep strains observed at constant stress need further investigation. With our current understanding of the behavior of brittle rocks it is not possible to predict the time to failure from observed creep strain rates. Estimates of time to failure based on these parameters can vary by more than four orders of magnitude. Therefore, it is necessary to conduct additional tests to define the critical parameters that control the long term behavior and strength of TSw2 tuff under repository conditions.

5.0 REFERENCES

- American Society for Testing and Materials, ASTM D4406-93, "Standard Test Method for Creep of Cylindrical Rock Core Specimens in Triaxial Compression", American Society for Testing and Materials, Philadelphia, PA, 1993.
- Boyd, P.J., R.J. Martin, III, and R.H. Price, "An Experimental Comparison of Laboratory Techniques in Determining Bulk Properties of Tuffaceous Rocks", SAND92-0119, Sandia National Laboratories, Albuquerque, NM, 1994.
- Brace, W.F., B.W. Paulding, Jr., and C.H. Scholz, "Dilatancy in the Fracture of Crystalline Rocks", *Journal of Geophysical Research*, 71(16), p. 3939-3953, 1966.
- Brechtel, C.E., M. Lin, E. Martin, and D.S. Kessel, "Geotechnical Characterization of the North Ramp of the Exploratory Studies Facility. Volume II of II NRG Corehole Data Appendices", SAND95-0488/2, Sandia National Laboratories, Albuquerque, NM, 1995.
- Charles, R.J., "The Strength of Silicate Glasses and Some Crystalline Oxides, In: Fracture, Proceedings of an International Conference on the Atomic Mechanisms of Fracture", B.L. Averbach, D.K. Felbeck, G.T. Hahn, and D.A. Thomas (eds.), John Wiley & Sons, New York, p. 225-249, 1959.
- Dunning, J.D., W.L. Lewis, and D.E. Dunn, "Chemomechanical Weakening in the Presence of Surfactants", *Journal of Geophysical Research*, 85(10), p. 5344-5354, 1980.
- Kicker, D.C., E.R. Martin, C.E. Brechtel, C.A. Stone, and D.S. Kessel, "Geotechnical Characterization for the Main Drift of the Exploratory Studies Facility", SAND95-2183, Sandia National Laboratories, Albuquerque, NM, 1997.
- Martin, R.J., III, "Time-Dependent Crack Growth in Quartz and Its Application to the Creep of Rocks", *Journal of Geophysical Research*, 77(8), p. 1406-1419, 1972.
- Martin, R.J., III, and W.B. Durham, "Mechanisms of Crack Growth in Quartz", *Journal of Geophysical Research*, 80(35), p. 4837-4844, 1975.
- Martin, R.J., III, P.J. Boyd, J.S. Noel, and R.H. Price, "Procedure Development Study: Low Strain Rate and Creep Experiments", SAND91-0527, Sandia National Laboratories, Albuquerque, NM, 1991.
- Martin, R.J., III, R.H. Price, P.J. Boyd, and J.S. Noel, "Creep in Topopah Spring Member Welded Tuff", SAND94-2585, Sandia National Laboratories, Albuquerque, NM, 1995.
- Ortiz, T.S., R.L. Williams, F.B. Nimick, B.C. Whittet, and D.L. South, "A Three-Dimensional Model of Reference Thermal-Mechanical and Hydrological Stratigraphy at Yucca Mountain, Southern Nevada", SAND84-1076, Sandia National Laboratories, Albuquerque, NM, 1985.
- Price, R.H., and S.J. Bauer, "Analysis of the Elastic and Strength Properties of Yucca Mountain Tuff, Nevada, In: Research & Engineering Applications in Rock Masses", Vol. 1, Proc. 26th U.S. Symposium on Rock Mechanics, Eileen Ashworth (ed.), A.A. Balkema, Boston, MA, p. 89-96, 1985.
- Wiederhorn, S.M., "Moisture Assisted Crack Growth in Ceramics", *International Journal of Fracture Mechanics*, 4(2), p. 171-177, 1968.

APPENDIX I

Information from the Reference Information Base Used in this Report

This report contains no information from the Reference Information Base.

Candidate Information for the Reference Information Base

This report contains no information for the Reference Information Base.

Candidate Information for the Geographic Nodal Information Study and Evaluation System

This report contains candidate information for the Geographic Nodal Information Study and Evaluation System (GeNESIS) in Tables 1, 2, 3, and 4. The data have been submitted to the SNL Participant Data Archive (PDA) and are indexed in the Automated Technical Data Tracking system (ATDT). The data packages have the following Data Tracking Numbers (DTN): SNL02030193001.016, SNL02030193001.017, SNL02030193001.018, and SNL02030193001.019, and SNL02030193001.020.

**YUCCA MOUNTAIN SITE CHARACTERIZATION PROJECT
SAND95-1759 - DISTRIBUTION LIST**

1	D. A. Dreyfus (RW-1) Director OCRWM US Department of Energy 1000 Independence Avenue SW Washington, DC 20585	1	Director, Public Affairs Office c/o Technical Information Resource Center DOE Nevada Operations Office US Department of Energy P.O. Box 98518 Las Vegas, NV 89193-8518
1	L. H. Barrett (RW-2) Acting Deputy Director OCRWM US Department of Energy 1000 Independence Avenue SW Washington, DC 20585	8	Technical Information Officer DOE Nevada Operations Office US Department of Energy P.O. Box 98518 Las Vegas, NV 89193-8518
1	S. Rousso (RW-40) Office of Storage and Transportation OCRWM US Department of Energy 1000 Independence Avenue SW Washington, DC 20585	1	J. R. Dyer, Deputy Project Manager Yucca Mountain Site Characterization Office US Department of Energy P.O. Box 30307 MS 523 Las Vegas, NV 89036-0307
1	R. A. Milner (RW-30) Office of Program Management and Integration OCRWM US Department of Energy 1000 Independence Avenue SW Washington, DC 20585	1	S. A. Orrell Laboratory Lead for YMP M&O/Sandia National Laboratories 1180 Town Center Dr. Las Vegas, NV 89134
1	D. R. Elle, Director Environmental Protection Division DOE Nevada Field Office US Department of Energy P.O. Box 98518 Las Vegas, NV 89193-8518	1	J. A. Canepa Laboratory Lead for YMP EES-13, Mail Stop J521 M&O/Los Alamos National Laboratory P.O. Box 1663 Los Alamos, NM 87545
1	T. Wood (RW-14) Contract Management Division OCRWM US Department of Energy 1000 Independence Avenue SW Washington, DC 20585	1	Repository Licensing & Quality Assurance Project Directorate Division of Waste Management, MS T7J-9 US NRC Washington, DC 20555
4	Victoria F. Reich, Librarian Nuclear Waste Technical Review Board 1100 Wilson Blvd., Suite 910 Arlington, VA 22209	1	Senior Project Manager for Yucca Mountain Repository Project Branch Division of Waste Management, MS T7J-9 US NRC Washington, DC 20555
1	Wesley Barnes, Project Manager Yucca Mountain Site Characterization Office US Department of Energy P.O. Box 30307 MS 523 Las Vegas, NV 89036-0307	1	NRC Document Control Desk Division of Waste Management, MS T7J-9 US NRC Washington, DC 20555

1	Chad Glenn NRC Site Representative 301 E Stewart Avenue, Room 203 Las Vegas, NV 89101	1	B. T. Brady Records Specialist US Geological Survey MS 421 P.O. Box 25046 Denver, CO 80225
1	Center for Nuclear Waste Regulatory Analyses Southwest Research Institute 6220 Culebra Road Drawer 28510 San Antonio, TX 78284	1	M. D. Voegelé Deputy of Technical Operations M&O/SAIC 1180 Town Center Dr. Las Vegas, NV 89134
2	W. L. Clarke Laboratory Lead for YMP M&O/ Lawrence Livermore Nat'l Lab P.O. Box 808 (L-51) Livermore, CA 94550	2	A. T. Tamura Science and Technology Division OSTI US Department of Energy P.O. Box 62 Oak Ridge, TN 37831
1	Robert W. Craig Technical Project Officer US Geological Survey 1180 Town Center Dr. Las Vegas, NV 89134	1	P. J. Weeden, Acting Director Nuclear Radiation Assessment Div. US EPA Environmental Monitoring Sys. Lab P.O. Box 93478 Las Vegas, NV 89193-3478
1	J. S. Stuckless, Senior Science Advisor MS 425 Yucca Mountain Project Branch US Geological Survey P.O. Box 25046 Denver, CO 80225	1	John Fordham, Deputy Director Water Resources Center Desert Research Institute P.O. Box 60220 Reno, NV 89506
1	L. D. Foust, Asst. General Mgr. Nevada Site TRW Environmental Safety Systems 1180 Town Center Dr. Las Vegas, NV 89134	1	The Honorable Jim Regan Chairman Churchill County Board of Commissioners 10 W. Williams Avenue Fallon, NV 89406
1	A. L. Flint U. S. Geological Survey 1180 Town Center Dr. Las Vegas, NV 89134	1	R. R. Loux Executive Director Agency for Nuclear Projects State of Nevada Evergreen Center, Suite 252 1802 N. Carson Street Carson City, NV 89710
1	Robert L. Strickler Vice President & General Manager TRW Environmental Safety Systems, Inc. 2650 Park Tower Dr. Vienna, VA 22180	1	Brad R. Mettam Inyo County Yucca Mountain Repository Assessment Office P. O. Drawer L Independence, CA 93526
1	Jim Krulik, Technical Program Officer US Bureau of Reclamation Code D-8322 P.O. Box 25007 Denver, CO 80225-0007	1	Vernon E. Poe Office of Nuclear Projects Mineral County P.O. Box 1600 Hawthorne, NV 89415

1	Les W. Bradshaw Program Manager Nye County Nuclear Waste Repository Project Office P.O. Box 1767 Tonopah, NV 89049	1	Library Acquisitions Argonne National Laboratory Building 203, Room CE-111 9700 S. Cass Avenue Argonne, IL 60439
1	Florindo Mariani White Pine County Coordinator P. O. Box 135 Ely, NV 89301	1	Glenn Van Roekel Manager, City of Caliente P.O. Box 158 Caliente, NV 89008
1	Tammy Manzini Lander County Yucca Mountain Information Officer P.O. Box 10 Austin, NV 89310	1	G. S. Bodvarsson Head, Nuclear Waste Department Lawrence Berkeley National Laboratory 1 Cyclotron Road, MS 50E Berkeley, CA 94720
1	Jason Pitts Lincoln County Nuclear Waste Program Manager P. O. Box 158 Pioche, NV 89043	1	Steve Hanauer (RW-2) OCRWM U. S. Department of Energy 1000 Independence Ave. Washington, DC 20585
1	Dennis Bechtel, Coordinator Nuclear Waste Division Clark County Dept. of Comprehensive Planning P.O. Box 55171 Las Vegas, NV 89155-1751	5	Randolph J. Martin III New England Research 76 Olcott Drive White River, VT 05001
1	Juanita D. Hoffman Nuclear Waste Repository Oversight Program Esmeralda County P.O. Box 490 Goldfield, NV 89013	1	Robert W. Clayton M&O/WCFS 1180 Town Center Drive Las Vegas, NV 89134
1	Sandy Green Yucca Mountain Information Office Eureka County P.O. Box 714 Eureka, NV 89316	1	Richard C. Quitmeyer M&O/WCFS 1180 Town Center Drive Las Vegas, NV 89134
1	Economic Development Dept. City of Las Vegas 400 E. Stewart Avenue Las Vegas, NV 89101	1	Mark C. Tynan DOE/YMPSCO 1180 Town Center Drive MS 523/HL Las Vegas, NV 89134
1	Community Planning & Development City of North Las Vegas P.O. Box 4086 North Las Vegas, NV 89030	2	MS 1330 K. Hart, 6811 100/1.2.3.2.7.1.3/SAND95- 1759/QA
2	Librarian YMP Research & Study Center 1180 Town Center Dr. Las Vegas, NV 89134	20	1330 WMT Library, 6752
		1	9018 Central Technical Files, 8940-5
		5	0899 Technical Library, 4414
		2	0619 Review and Approval Desk, 12690, For DOE/OSTI
		15	1325 R. H. Price, 6811
		5	0751 N. Brodsky, 6117
		1	0751 L. S. Costin, 6117
		5	1399 D. S. Kessel, 6850